Journal of
Medicinal Chemistry

Article

Syntheses and Evaluation of New Bisacridine Derivatives for Dual Binding of G-Quadruplex and i-Motif in Regulating Oncogene c-myc Expression

Guo-Tao Kuang, Meiling Zhang, Shuangshuang Kang, Dexuan Hu, Xiaoya Li, Zuzhuang Wei, Xue Gong, Lin-Kun An, Zhi-Shu Huang, Bing Shu, and Ding Li

J. Med. Chem., **Just Accepted Manuscript** • DOI: 10.1021/acs.jmedchem.9b01917 • Publication Date (Web): 12 Aug 2020

Just Accepted

is published by the American Chemical Society. 1155 Sixteenth Street N.W., Washington, DC 20036

Syntheses and Evaluation of New Bisacridine Derivatives for Dual Binding of G-Quadruplex and i-Motif in Regulating Oncogene *c-myc* Expression

Guotao Kuang[1], Meiling Zhang[1], Shuangshuang Kang[1], Dexuan Hu[1], Xiaoya Li[1], Zuzhuang Wei[1], Xue Gong[1], Lin-Kun An[1], Zhi-Shu Huang[1], Bing Shu[1,2,*], and Ding Li[1,*]

[1]School of Pharmaceutical Sciences, Sun Yat-sen University, 132 Waihuan East Road, Guangzhou 510006, PR China

[2]School of Pharmacy, Guangdong Pharmaceutical University, Guangzhou 510006, PR China

* Corresponding author.

Ding Li, Tel: 8620 3994 3058; E-mail: liding@mail.sysu.edu.cn;

Bing Shu, Tel: 8620 3935 2129; E-mail: shubing@gdpu.edu.cn.

Abstract

c-myc oncogene is an important regulator for cell growth and differentiation, and its aberrant overexpression is closely related to the occurrence and development of various cancers. Thus, suppression of *c-myc* transcription and expression has been investigated for cancer treatment. In this study, various new bisacridine derivatives were synthesized and evaluated for their binding with *c-myc* promoter G-quadruplex and i-motif. We found that **a9** could bind to and stabilize both G-quadruplex and i-motif resulting in down-regulation of *c-myc* gene transcription. **a9** could inhibit cancer cell proliferation, and induce SiHa cell apoptosis and cycle arrest. **a9** exhibited tumor growth inhibition activity in SiHa xenograft tumor model, which might be related to its binding with *c-myc* promoter G-quadruplex and i-motif. Our results suggested that **a9** as a dual G-quadruplex/i-motif binder could be effective on both oncogene replication and transcription, and become a promising lead compound for further development with improved potency and selectivity.

KEY WORDS: bisacridine; *c-myc*; G-quadruplex; i-motif; cancer

INTRODUCTION

The human *c-myc* proto-oncogene is an important regulator of a wide array of cellular processes necessary for cell growth and differentiation, and its dysregulation is one of the hallmarks of many cancers.[1-4] The aberrant overexpression of *c-myc* gene is closely related to the occurrence and development of various human cancers.[3, 5] Therefore, the strategies for suppression of *c-myc* transcription and prevention of C-MYC protein from binding to its relative proteins or genes in established cancer cell lines have been well studied for cancer treatment.[3-4, 6-9] It has been shown that the crystal structure of C-MYC protein does not have a cavity that permit small molecules binding easily, so that it is very complicated to simulate and design direct inhibitors.[9-10] Thus, the development of effective methods for down-regulating *c-myc* gene transcription by genetic silencing has become practical and promising therapeutic strategies.[11]

The nuclease hypersensitive element III_1 (NHE III_1), located at upstream from the P1 promoter of *c-myc* gene, controls 85-90% of *c-myc* transcription.[4, 12-13] The region is guanine/cytosine rich (GC-rich) and contains two nuclease hypersensitive sites. As a result of transcription induced negative superhelicity during cellular processes, GC-rich region can open up to make the formation of two non-B-form unique DNA secondary structures: G-quadruplexes on the G-rich strand and i-motif on the complementary C-rich strand.[13-15] The *c-myc* promoter G-quadruplexes have been largely focused and previously characterized to play key roles as transcriptional repressors in modulating gene transcription, and various ligands binding to and inducing the formation of *c-myc* promoter G-quadruplex could suppress *c-myc* gene transcription and expression.[12, 16-17] The population of G−quadruplexes have been found to be the lowest at cell

cycle stage G0/G1 (no replication), intermediate at G1/S and maximal during S phase (DNA replication) by using antibody staining, consistent with cellular replication dependent formation of G−quadruplexes.[18] It should be noted that G-rich sequences are widely existed in promoter regions of human genome, which could be folded into G-quadruplexes. Therefore, selective recognition and stabilization of small molecule binding ligands is a problem. One possible solution is to have their corresponding C-rich strands in consideration, which could form i-motif structures and influence stability of corresponding G-quadruplexes.

However, the studies of i-motif structures are rarely reported. The *c-myc* gene promoter C-rich strand at NHE III_1 region could form i-motif structure, which comprises two parallel duplexes with intercalated hemiprotonated cytosine$^+$-cytosine (C^+-C) base pairs.[6, 19-20] The i-motif structure can form under slightly acidic condition or at neutral pH under molecular crowding condition, and it is more complex than the G-quadruplex in the complementary strand.[21-25] Recent studies suggest the existence of i-motif structure in cells and its important roles in gene regulation, which also make it an attractive target for anticancer drug development and gene regulation processes.[19, 22-23, 25-28] Besides, the formation of i-motifs varied over the cell cycle, with the highest level of formation occurring during late G1 phase, which is characterized by high levels of transcription and cellular growth. This is significantly different from G−quadruplex formation, which occurs predominately during the DNA replication S phase, suggesting that the occurrence of i-motifs and G-quadruplexes are generally independent, and the i-motifs regulation in cell cycle might be more important than the G−quadruplexes regulation.[27] In addition, it has been shown that i-motifs are better replication inhibitors than mixed-type G-quadruplexes or hairpin structures, even though all

of them have similar thermodynamic stabilities.[29] To date, several i-motif binding ligands have been characterized, including **porphyrin** (**TMPYP4**),[30-31] **PBP1-2**,[32] **acridone**,[33] **phenanthroline**[34] and **mitoxantrone**[6] (**Figure 1**). It has been reported that **PBP1** could bind to and induce the formation of *bcl-2* promoter i-motif to up-regulate gene transcription and expression. In comparison, **PBP2** could bind to and induce the formation of *bcl-2* promoter G-quadruplex and down-regulate gene transcription and expression. In a previous study, we have reported that an **acridone** derivative could selectively bind to and induce *c-myc* promoter i-motif formation, resulting in down-regulation of *c-myc* transcription. These findings indicated that *c-myc* promoter i-motif could play an important role as a transcriptional regulator in *c-myc* gene transcription. It should be noted that drug resistance could happen if a molecule binds to only one molecular target, and therefore a multi-functional molecule binding to more than one target especially in different phases of cell cycle could overcome drug resistance and become much effective. Presently, small molecules binding to both *c-myc* promoter G-quadruplex (cellular S phase arrested) and i-motif (late G1 phase interfered) could be much efficient in down-regulating gene transcription with improved selectivity.

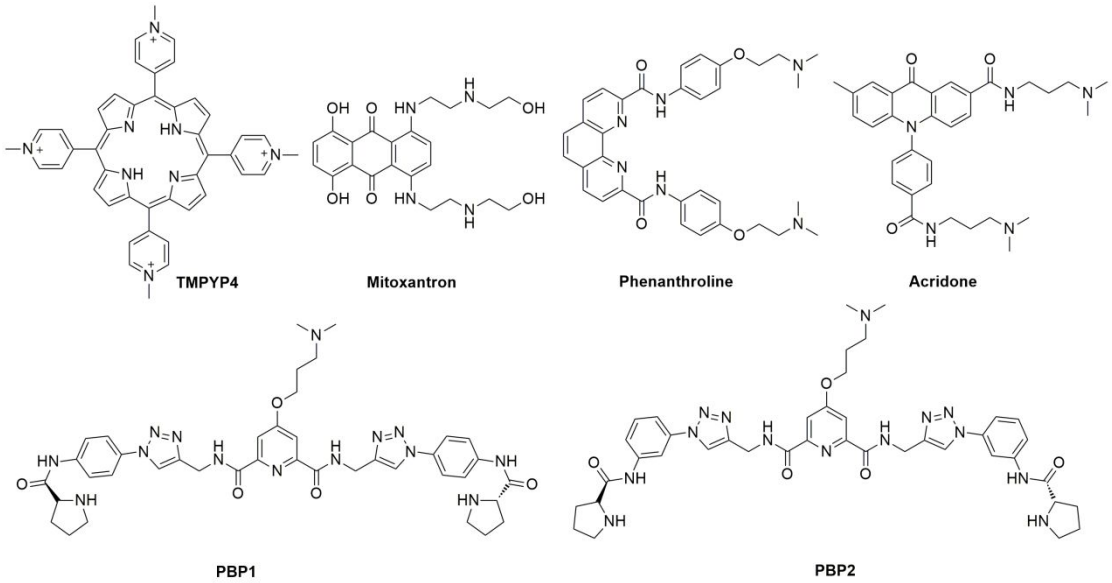

Figure 1. The structures of **TMPYP4**, **mitoxantrone**, **phenanthroline**, **acridone**, and **PBP1-2**.

In order to find small molecular ligands targeting both *c-myc* promoter G-quadruplex and i-motif structures, we screened our synthesized compounds library in our laboratory by using FRET-melting assay. We found that an acridine derivative could stabilize both *c-myc* promoter G-quadruplex and i-motif structures. Then, we designed and synthesized a variety of structural analogs and derivatives, and found that a bisacridine derivative (**a5**) could increase the stability of both G-quadruplex and i-motif, with decreased stability to duplex and hairpin structures. We further synthesized **24** bisacridine analogs and evaluated their stability and binding affinity to both G-quadruplex and i-motif. Among these compounds, **a9** was found to be a potent dual binding ligand stabilizing both *c-myc* promoter G-quadruplex and i-motif. Our *in vitro* and cellular experiments confirmed that **a9** could interact with both G-quadruplex and i-motif structures. Our further studies suggested that **a9** could hinder cell migration and repress tumor growth possibly through down-regulating *c-myc* gene transcription. These findings illustrated that stabilization of

both *c-myc* promoter G-quadruplex and i-motif structures with **a9** could repress *c-myc* gene transcription and expression much effectively and selectively, which could offer a significantly improved strategy for controlling tumor cells growth and migration.

RESULTS AND DISCUSSION

Screening of small molecules for binding to *c-myc* promoter G-quadruplex and i-motif. In order to study dual G-quadruplex/i-motif interactive compounds, fluorescence resonance energy transfer (FRET) melting experiment was performed to screen our compounds library containing about 80 compounds, including acridone derivatives, quinoline derivatives, acridine derivatives, and imidazole derivatives (supporting information, **Figure S1**), with dual labeled DNA oligomer containing fluorophores at both 5′-end and 3′-end (**Table S1**). Compounds that could increase the melting temperature (ΔT_m) for more than 5 °C were considered as potential hits. We found that quinoline derivatives, imidazole derivatives, indole derivatives and acridone derivatives (**B01-12**) did not significantly increase the melting temperatures of i-motif or G-quadruplex. Acridone derivatives (**B13-24**) could stabilize *c-myc* promoter i-motif more significantly than G-quadruplex. Acridine derivatives (**AD01-16**) could increase the stability of both G-quadruplex and i-motif, which were regarded as hit compounds in the present study (**Figure S1**). Among these acridine derivatives, N^1-(2,7-dimethylacridin-9-yl)-N^2,N^2-dimethylethane-1,2-diamine (**AD06**) could significantly stabilize both *c-myc* promoter G-quadruplex and i-motif structures with its ΔT_m values of 8.3 °C and 10.0 °C respectively at 5 μM concentration. However, **AD06** could also stabilize hairpin structure with ΔT_m value of 6.8 °C, indicating its possible DNA intercalative

effect. It has been reported that a molecule containing two acridine units connected with a linker of two diethylenetriamines (named as **BisA**) could increase the melting temperatures of the G-quadruplex and i-motif much more significantly than a monomeric acridine substituted with two propylaminomethyl groups (named as **MonoA)**.[35] This result indicated that two or more pharmacophores connected with a single chain amine linker could have higher binding affinity, possibly through increased molecular interactions. Therefore, we designed and synthesized a new compound having two acridine units connected with a single chain amine linker (**BisA01**). We found that **BisA01** could stabilize both G-quadruplex and i-motif with the ΔT_m values of 6.2 and 16.0 ^oC, respectively. In comparison, **BisA01** had decreased stability to hairpin structure (ΔT_m = 2.5 ^oC), indicating that **BisA01** might have less intercalative effect to double strand DNA possibly due to its increased molecular size. This could increase the selectivity of the hit compound for G-quadruplex and i-motif with relatively less side effect or toxicity. These inspiring data encouraged us to further synthesize **BisA01** analogs for optimizing the activity.

Syntheses of bisacridine derivatives. Since **BisA01** was found as a hit compound with dual G-quadruplex/i-motif binding affinity and improved selectivity, we further synthesized various analogs for optimizing binding interactions with the G-quadruplex and i-motif. The two acridine rings of **BisA01** could possibly stack on the external 5′-terminal G-quartet through π-π stacking interactions, or interact with the loops of G-quadruplex/i-motif. The linker of two acridine rings could interact with the grooves of G-quadruplex/i-motif through electrostatic interactions with negatively charged phosphate diester backbone. Besides, polyamine chains could facilitate

molecular entrances for their optimal delivery to target via polyamine transport system (PTS), especially for drugs interacting with DNA, to produce cellular DNA damage and cell apoptosis.[36-38] In the present study, we designed and synthesized various bisacridine derivatives linked with different amine chains (**a5-24**), as shown in **Figure 2** and **Scheme I**. It should be mentioned that several i-motif binding ligands have substituted amine side chains as shown in **Figure 1**, which could increase their stability and binding affinity to promoter i-motif. We have previously reported that acridone derivatives linked with benzoyl amine side chains had increased binding affinity to *c-myc* promoter i-motif. Thus, in the present study we introduced two benzoyl amine side chains to bisacridine derivatives for compounds **a25-26**. For comparison, we introduced two ester groups to bisacridine derivatives for compounds **a27-28**.

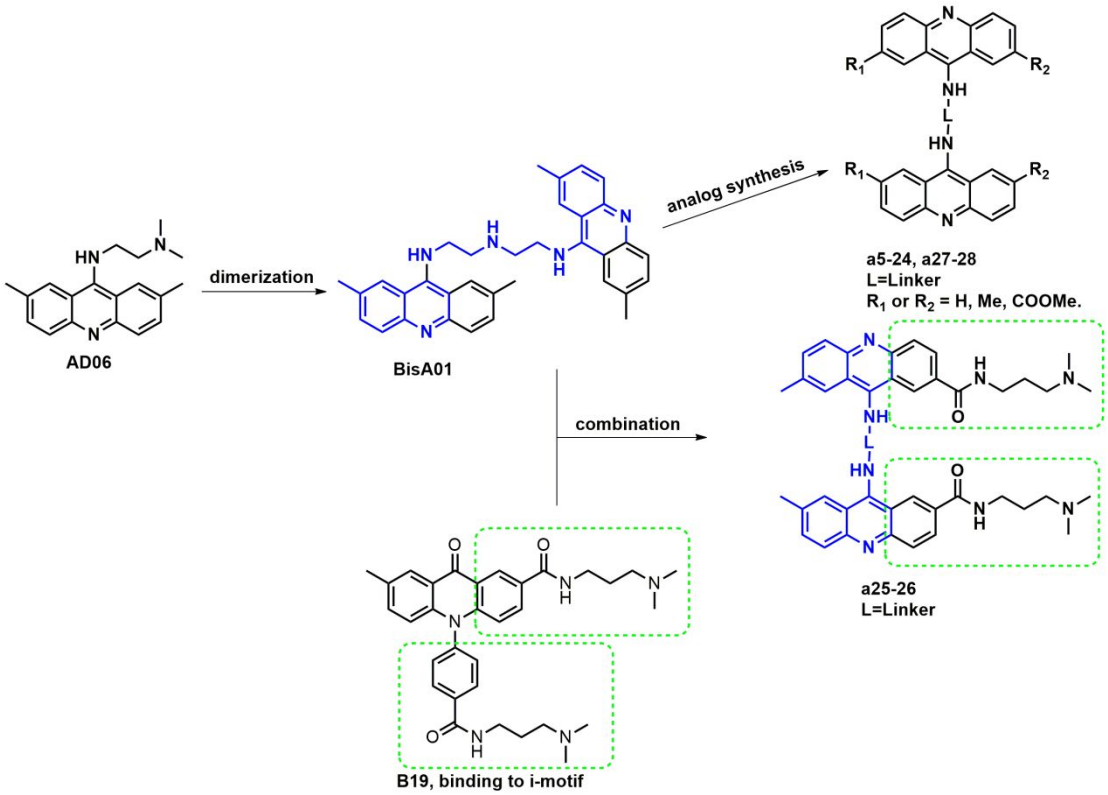

Figure 2. Modification strategies of the bisacridine derivatives scaffold.

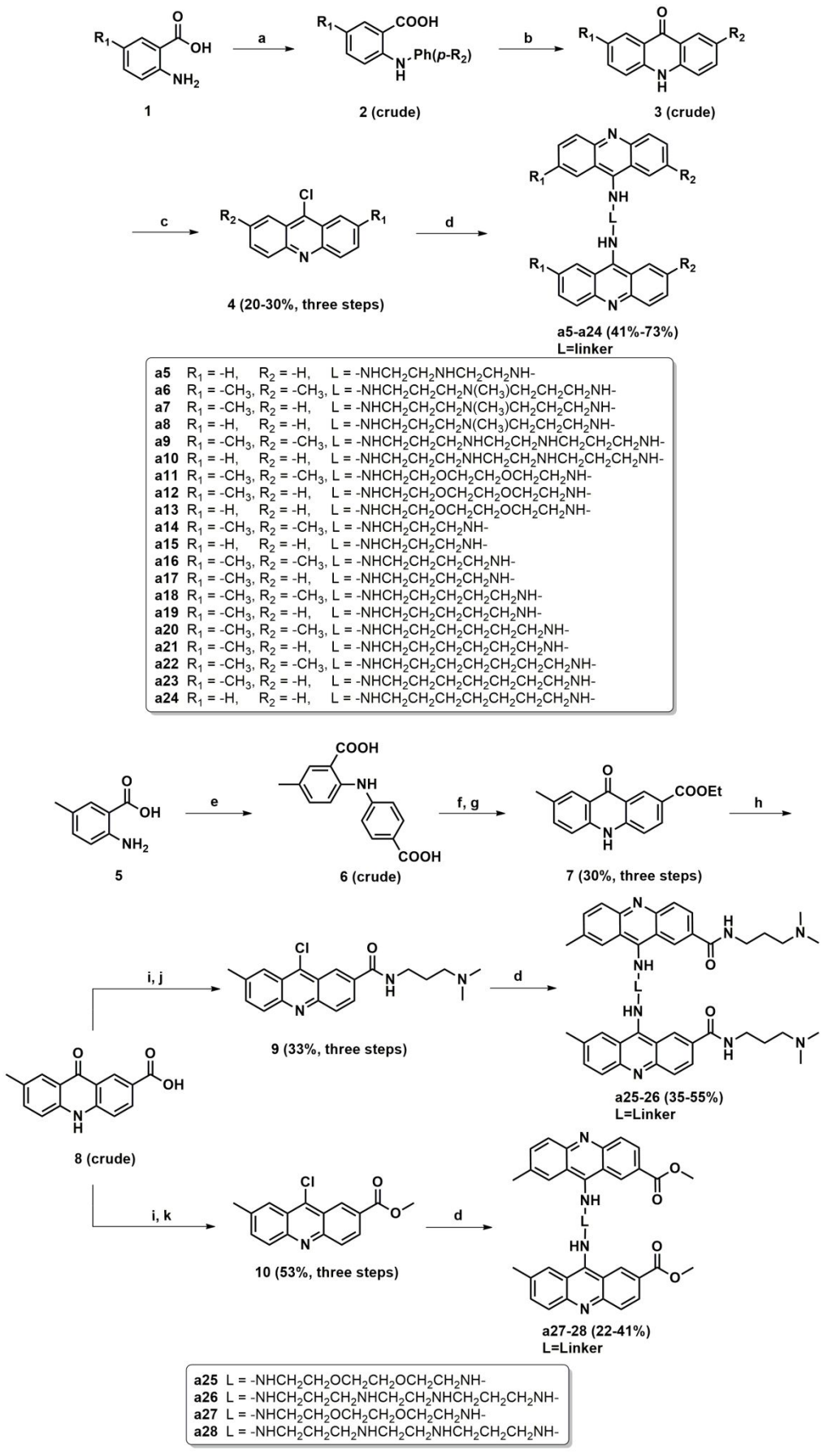

a5 R_1 = -H, R_2 = -H, L = -$NHCH_2CH_2NHCH_2CH_2NH$-
a6 R_1 = -CH_3, R_2 = -CH_3, L = -$NHCH_2CH_2CH_2N(CH_3)CH_2CH_2CH_2NH$-
a7 R_1 = -CH_3, R_2 = -H, L = -$NHCH_2CH_2CH_2N(CH_3)CH_2CH_2CH_2NH$-
a8 R_1 = -H, R_2 = -H, L = -$NHCH_2CH_2CH_2N(CH_3)CH_2CH_2CH_2NH$-
a9 R_1 = -CH_3, R_2 = -CH_3, L = -$NHCH_2CH_2CH_2NHCH_2CH_2NHCH_2CH_2CH_2NH$-
a10 R_1 = -H, R_2 = -H, L = -$NHCH_2CH_2CH_2NHCH_2CH_2NHCH_2CH_2CH_2NH$-
a11 R_1 = -CH_3, R_2 = -CH_3, L = -$NHCH_2CH_2OCH_2CH_2OCH_2CH_2NH$-
a12 R_1 = -CH_3, R_2 = -H, L = -$NHCH_2CH_2OCH_2CH_2OCH_2CH_2NH$-
a13 R_1 = -H, R_2 = -H, L = -$NHCH_2CH_2OCH_2CH_2OCH_2CH_2NH$-
a14 R_1 = -CH_3, R_2 = -CH_3, L = -$NHCH_2CH_2CH_2NH$-
a15 R_1 = -H, R_2 = -H, L = -$NHCH_2CH_2CH_2NH$-
a16 R_1 = -CH_3, R_2 = -CH_3, L = -$NHCH_2CH_2CH_2CH_2NH$-
a17 R_1 = -CH_3, R_2 = -H, L = -$NHCH_2CH_2CH_2CH_2NH$-
a18 R_1 = -CH_3, R_2 = -CH_3, L = -$NHCH_2CH_2CH_2CH_2CH_2NH$-
a19 R_1 = -CH_3, R_2 = -H, L = -$NHCH_2CH_2CH_2CH_2CH_2NH$-
a20 R_1 = -CH_3, R_2 = -CH_3, L = -$NHCH_2CH_2CH_2CH_2CH_2CH_2NH$-
a21 R_1 = -CH_3, R_2 = -H, L = -$NHCH_2CH_2CH_2CH_2CH_2CH_2NH$-
a22 R_1 = -CH_3, R_2 = -CH_3, L = -$NHCH_2CH_2CH_2CH_2CH_2CH_2CH_2NH$-
a23 R_1 = -CH_3, R_2 = -H, L = -$NHCH_2CH_2CH_2CH_2CH_2CH_2CH_2NH$-
a24 R_1 = -H, R_2 = -H, L = -$NHCH_2CH_2CH_2CH_2CH_2CH_2CH_2NH$-

a25 L = -$NHCH_2CH_2OCH_2CH_2OCH_2CH_2NH$-
a26 L = -$NHCH_2CH_2CH_2NHCH_2CH_2NHCH_2CH_2CH_2NH$-
a27 L = -$NHCH_2CH_2OCH_2CH_2OCH_2CH_2NH$-
a28 L = -$NHCH_2CH_2CH_2NHCH_2CH_2NHCH_2CH_2CH_2NH$-

Scheme I. Reagents and conditions: (a) 1-bromo-4-substituted-benzene, Cu, CuI, K_2CO_3, DMF, 120 °C, 12 h; (b) conc. H_2SO_4, 100 °C, 2 h; (c) $POCl_3$, 100 °C, 3 h (20-30% yield for three steps); (d) NH_2-L-NH_2, PhOH, 100 °C, 8 h (yield 22-73%); (e) Cu, K_2CO_3, DMF, 120 °C, 12 h; (f) conc. H_2SO_4, 140 °C, 4 h; (g) EtOH, 80 °C, 2 h (30% yield for three steps); (h) MeOH, 10% NaOH, 60 °C, 1 h; (i) $SOCl_2$, 60 °C, 1 h; (j) DCM, TEA, N^1,N^1-dimethylpropane-1,3-diamine, 0 °C, 1 h (33% yield for three steps); (k) DCM, TEA, MeOH, 0 °C, 1h (53% yield for three steps).

The synthetic pathway for bisacridine derivatives **a5-28** is shown in **Scheme 1**. Benzoic acid **1** as starting material was reacted with bromobenzene to give intermediate **2** as a crude mixture, which was used for next step without purification. The intermediate **2** reacted in concentrated sulfuric acid through Friedel-Crafts acylation reaction to produce intermediate acridone **3**, which was then reacted with phosphorus oxychloride immediately to generate acridine derivative **4**. Besides, crude intermediate **6** was obtained through reaction of benzoic acid **5** with 4-bromobenzoic acid instead of bromobenzene in a similar condition, which was followed with intra-cyclization reaction in concentrated sulfuric acid, and then reaction with ethanol to generate acridone **7**. The intermediate **7** was hydrolyzed to give an acid **8** under basic condition, followed by treatment of $SOCl_2$ to generate its acyl chloride, and then reaction with N^1,N^1-dimethylpropane-1,3-diamine or MeOH to give key intermediates **9** and **10**, respectively. At last, the acridine intermediates **4**, **9**, **10** reacted with NH_2-L-NH_2 in phenol to give the target compounds **a5-28**. All synthesized intermediates and compounds were purified and their structures were determined by using HPLC, NMR and HRMS. The purified compounds **a5-28**

were used for subsequent biophysical and biochemical as well as cell-based studies.

Structure-activity relationship studies. The binding affinities of the synthesized bisacridine derivatives for *c-myc* promoter G-quadruplex and i-motif were studied through FRET-melting experiment to evaluate their thermal stability changes, and the results were shown in **Table 1** and **Figure S2**. All synthesized bisacridine derivatives with long alkyl amine linker could increase the stability of *c-myc* promoter G-quadruplex (FPu22T) with ΔT_m values ranged from 7.7 to 17.1 °C. Among these bisacridine derivatives, **a6-10** with relatively long alkyl amine linker could increase melting temperature (4.5-11.8 °C) of *c-myc* promoter i-motif (FPy33T), suggesting that long alkyl amine linker could be a favorable factor. **a25-26** with benzoyl amide side chains could also increase melting temperature of *c-myc* promoter i-motif with ΔT_m values of 27.4 and 24.3 °C, respectively. It is possible that the benzoyl amide side chains could participate in hydrogen bonding interactions with the i-motif to increase stabilization.[33]

Table 1 . Melting temperature changes for oligomers determined through FRET-melting experiment

Comp.	ΔTm (°C)[a]			Comp.	ΔTm (°C)		
	FPy33T	FPu22T	F10T		FPy33T	FPu22T	F10T
a5	0.7	15.2	2.5	**a19**	0.2	11.4	1.9
a6	4.5	15.6	3.8	**a20**	10.1	16.8	2.7
a7	6.4	12.1	6.2	**a21**	1.2	10.0	1.7
a8	7.3	7.7	10.8	**a22**	1.4	15.7	1.8

a9	11.0	9.9	4.5	**a23**	3.4	15.3	3.6
a10	11.8	12.5	9.8	**a24**	0.6	8.8	9.3
a11	1.0	13.5	2.3	**a25**	27.4	8.3	2.2
a12	0.1	14.3	3.0	**a26**	24.3	17.1	2.8
a13	0.1	10.6	3.4	**a27**	1.0	14.3	2.5
a14	2.4	14.1	0.7	**a28**	2.0	8.6	4.8
a15	1.3	14.0	2.2	**AD06**	2.7	6.2	4.1
a16	9.1	10.4	0.8	**AD07**	1.3	0.8	3.3
a17	0.4	13.9	2.0	**AD08**	1.2	1.1	3.1
a18	1.0	11.0	2.7				

[a] ΔTm = Tm (DNA + ligand) - Tm (DNA). The concentrations of FPy33T, FPu22T and F10T were 0.2 μM, and the concentrations of compounds were 1.0 μM. The melting temperatures of FPy33T, FPu22T and F10T in the absence of compounds were 53.2 °C, 66.5 °C and 59.1 °C, respectively.

Then, we studied the binding affinity and selectivity of our synthesized bisacridine derivatives to *c-myc* promoter G-quadruplex and i-motif through SPR method. The binding constant K_D values for binding affinity of the bisacridine derivatives to G-quadruplex, i-motif, C-rich single stand oligomer, and hairpin were determined as shown in **Table 2 and Figure S3**. As a control experiment, their corresponding monomeric acridines with **AD06-08** as examples, showed no significant interaction with the DNA. All synthesized bisacridine derivatives with long alkyl

amine linkers could bind to G-quadruplex structure formed by Pu27 with K_D values ranged from 1.1 to 18.3 μM. Compounds **a5**, **a11-24** with relatively few amine functional groups on the linkers showed relatively weak i-motif binding affinity. Compounds **a6-10** with relatively more amine functional groups on the linkers could bind well to *c-myc* promoter i-motif with their K_D values ranged from 2.4 to 9.1 μM, suggesting that the amines on the linkers could be favorable for their binding affinity to *c-myc* promoter i-motif.

Table 2. The binding affinity of bisacridines **a5-28** to different DNA structures determined by using SPR

Comp.	K_D (μM)				Comp.	K_D (μM)			
	Py33 (i-motif)	Py33 (ssDNA)	Pu27	Duplex		Py33 (i-motif)	Py33 (ssDNA)	Pu27	Duplex
a5	12.3	-[a]	4.7	6.5	**a19**	14.5	26.1	16.3	-
a6	10.5	13.9	5.5	22.2	**a20**	12.4	4.7	1.1	-
a7	10.7	8.91	6.9	16.4	**a21**	25.1	-	14.3	-
a8	9.1	-	18.3	8.1	**a22**	-	8.8	6.1	10.7
a9	2.4	-	7.7	18.5	**a23**	-	-	10.3	24.8
a10	3.8	-	13.8	6.0	**a24**	-	14.7	11.6	7.4
a11	26.2	-	3.6	22.1	**a25**	8.5	-	3.7	17.4
a12	13.0	21.6	5.1	33.2	**a26**	1.0	-	2.7	21.7
a13	16.0	-	9.3	5.8	**a27**	10.3	2.9	1.4	12.5
a14	-	-	9.2	35.4	**a28**	3.8	-	2.9	11.8

a15	-	13.7	4.3	10.1	**AD06**	-	-	-	13.1
a16	16.0	6.8	2.9	-	**AD07**	-	-	-	-
a17	-	-	1.6	-	**AD08**	-	-	-	-
a18	-	23.7	7.3	33.6					

[a] No significant binding was found for the addition of up to 50 μM ligand, which might indicate no specific interaction between the ligand and the DNA.

Next, carboxyl amide side chains were introduced to compounds **a11** and **a9** to give **a25** and **a26**, which showed increased binding affinity to *c-myc* promoter i-motif with K_D values of 8.5 and 1.0 μM respectively, indicating their favorable effect for binding interactions with the i-motif. Besides, these compounds generally had relatively high binding affinity to *c-myc* promoter i-motif structure rather than C-rich single-stand oligonucleotide at pH 7.4 (**Table 2 and Figure S3**). In addition, we found that most bisacridine derivatives with various R^1 and R^2 substitutive groups showed relatively weak binding affinity to double-strand DNA. In comparison, **a5**, **a10**, **a13** and **a24** without substituent showed relatively high binding affinity to double-strand DNA. This might indicate that R^1 and R^2 substitutive groups could disturb their interactions with double-strand DNA. Generally, our structure-activity relationship data for their binding to G-quadruplex and i-motif were consistent with those for their stability to G-quadruplex and i-motif. Among our synthetic compounds, **a9** and **a26** exhibited much better binding affinity (**Table 2 and Figure S3**) than the hit compound **BisA01**. Our FRET and SPR results all showed that our bisacridine derivatives with substitutive groups had generally weak binding affinity and stability to duplex

DNA, indicating their insignificant intercalative effect compared with their binding affinity to *c-myc* promoter G-quadruplex/i-motif.

In-depth studies of selected bisacridine derivatives. On the basis of the above data, compounds **a9** and **a26** had relatively high *ΔTm* values and strong binding affinity, which were selected for further studies with other compounds as controls for comparison. Their interactions with G-quadruplex/i-motif were studied through circular dichroism (CD) spectroscopy, isothermal titration calorimetry (ITC), NMR, and native PAGE for further verification of these interactions.

CD spectroscopy has been used previously as a sensitive method to determine the effects of various ligands on the conformations of G-quadruplex/i-motif under different conditions.[6, 23] The oligomer Pu27 (**Table S1**) was used as the *c-myc* G-quadruplex forming sequence. As shown in **Figure 3A**, in the presence of 100 mM KCl, Pu27 showed a positive peak at 260-265 nm and a negative peak at near 240 nm, which suggested the formation of a typical parallel G-quadruplex structure. In the absence of potassium ion, its CD spectrum is similar to that in the presence of KCl, but with much lower signal intensity. After treatment with different bisacridine derivatives in the absence of potassium ion, we found that some compounds increased Pu27 CD signal intensity, while some others did not affect or decreased its signal intensity (**Figure S4**). Generally, the bisacridines with linker containing amine group, alkyl group or oxygen atom could maintain or increase the CD signal intensity, especially the derivatives with linker containing oxygen atom (**a11-13**, **a27**) (**Figure 3A**). This might indicate that these compounds could effectively induce the formation of parallel G-quadruplex formation in the absence of metal ion.

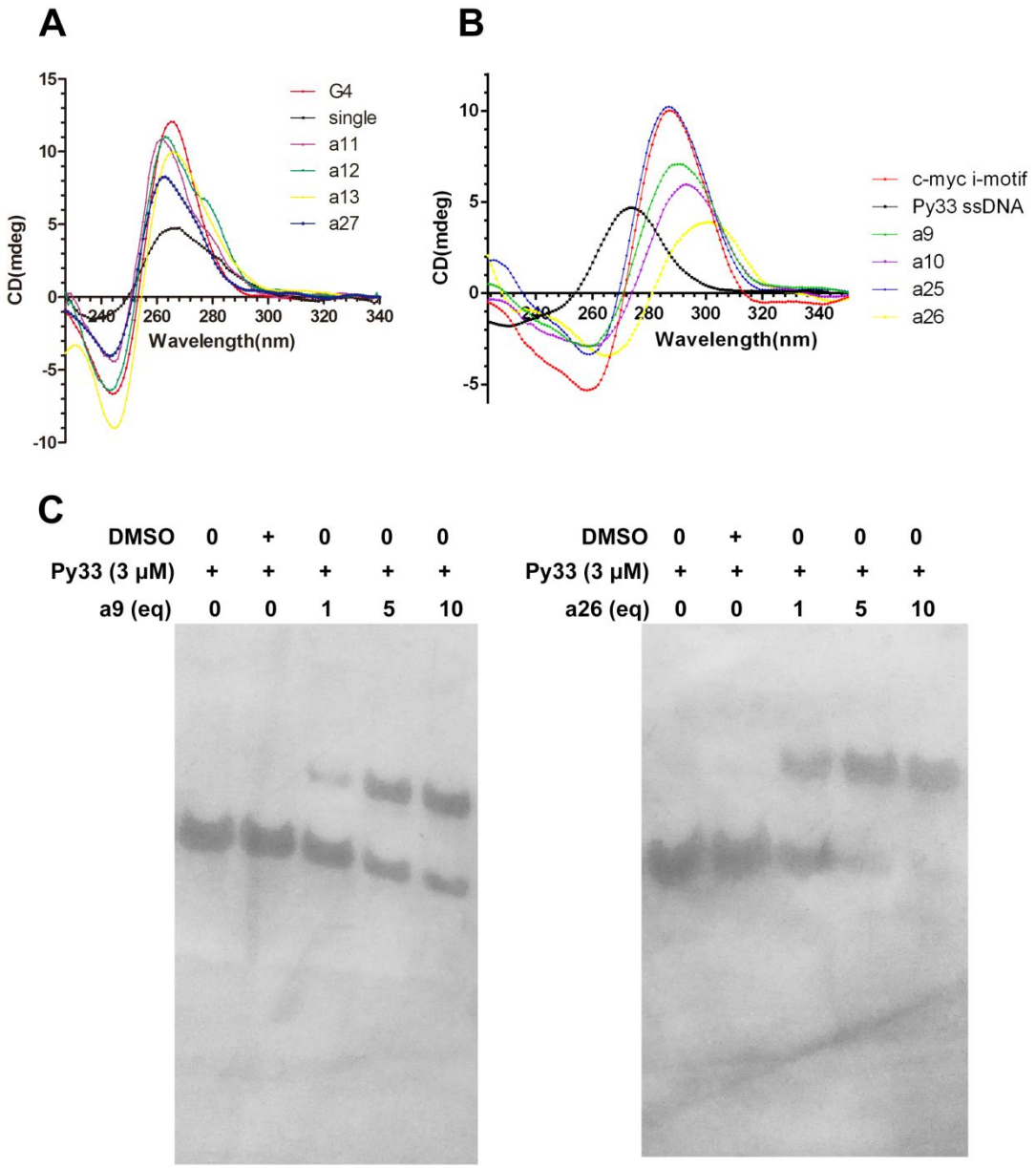

Figure 3. Interactions of the bisacridine derivatives to *c-myc* promoter G-quadruplex and i-motif. (A) CD spectra of Pu27 in 10 mM Tris-HCl buffer (pH 7.4) in the absence or presence of **a11-13**, and **a27**. (B) CD spectra of Py33 in the absence or presence of **a9-10**, **a25-26** at pH 5.5. (C) Native PAGE image analysis for concentration-dependent binding of **a9** or **a26** to Py33.

Then we also studied the effects of our bisacridines on *c-myc* promoter i-motif by using CD spectroscopy. Oligomer Py33 showed a positive peak at 287-290 nm and a negative peak at near 260 nm at pH 5.5, which indicated the formation of i-motif structure.[6, 23, 39] For comparison as a control at pH 7.0, the CD spectra exhibited the feature of random coil (blue) with only a positive peak at near 270 nm (**Figure 3B**).[40-43] **a9-10** and **a25-26** had relatively high stability and strong binding affinity to the i-motif, which decreased both positive peak at 288 nm and negative peak at 260 nm without switching to random coil characterized with 270 nm in the CD spectroscopy (**Figure 3B**), indicating that these compounds could cause some conformational change on *c-myc* promoter i-motif structure. We preformed CD melting experiment for **a9**, **a11**, and **a26**. Our results showed that **a9** and **a26** stabilized both G-quadruplex and i-motif, while **a11** stabilized G-quadruplex only **(Table S3, Figure S5)**, which were consistent with our FRET-melting result.

^{1}H NMR spectroscopy was also a common method to characterize conformation of G-quadruplex/i-motif structures.[14,39] We studied the effects of **a9** on *c-myc* promoter i-motif/G-quadruplex using ^{1}H NMR. The hemi-protonated C-C^{+} base pairs imino proton peaks of oligomer Py33 were at 15-16 ppm, which indicated the formation of *c-myc* promoter i-motif. Upon titration with increasing concentration of **a9,** the i-motif signals at 15-16 ppm were gradually increased (**Figure S6B**). This result showed that **a9** could induce formation of i-motif structure. The Hoogsteen hydrogen imino proton peaks of oligomer Pu27 were at 10.5-12 ppm, which indicated formation of G-quadruplex. Compound **a9** increased the G-quadruplex signal at 10.5-12 ppm (**Figure S6B**), indicating that **a9** could induce formation of G-quadruplex structure.

ITC was a method to determine binding affinity of two in-solution biomolecules.[44] Here, we

used ITC to study the binding of **a9** with *c-myc* promoter i-motif or G-quadruplex. As shown in **Figure S6A**, **a9** bound to *c-myc* promoter i-motif with a K_D value of 0.65 μM, and bound to *c-myc* promoter G-quadruplex with a K_D value of 0.81 μM. These results showed that **a9** bound tightly with *c-myc* promoter i-motif and G-quadruplex, which were consistent with our SPR result.

To further confirm the binding affinity of **a9** and **a26** to *c-myc* promoter i-motif, native PAGE electrophoresis experiments were performed, which have been previously used to study the binding interactions of ligands with i-motif structures.[14, 45] Oligonucleotide Py33 could form different DNA structures at different pH conditions. Generally, under weakly acidic conditions, Py33 could aggregate and fold into an i-motif DNA secondary structure, resulting in larger molecular tightness and redistribution of peripheral charge, mainly represented by positive charge located at the center of the i-motif, while negative charge lay in the phosphate backbone region, producing a slower migration band in native PAGE gel.[14] However, under nearly neutral conditions, Py33 could unfold into an unordered random coil, which migrated faster than i-motif. In the present study, Py33 was co-annealed with different concentrations of **a9** and **a26** in 1×BPES buffer (pH 6.6), and the obtained mixture samples were stored at 4 ^{o}C overnight, separated through electrophoreses, and then silver-stained. As shown in **Figure 3C**, after additions of increasing concentration of **a9** and **a26**, a slower migration band was formed in a dose-dependent manner, indicating that **a9** and **a26** could bind to Py33 and possibly induce its transformation from random coil to i-motif structure.

Furthermore, we studied the selectivity of **a9** on different G-quadruplex or i-motif structures by using CD-melting, UV titration and SPR experiment. The melting temperatures for promoter

i-motif or G-quadruplex oligomers from some other genes (*bcl-2*, *c-kit*, PDGF, telomere, VEGF) were determined in the presence and absence of **a9**. Compound **a9** exhibited the highest ΔT_m values for *c-myc* promoter i-motif and G-quadruplex in comparison with other oligomers (**Table S4, Figure S5**). Compound **a9** also exhibited the lowest K_D value for *c-myc* promoter i-motif and G-quadruplex measured through UV titration and SPR experiment, indicating good binding selectivity of **a9** to *c-myc* promoter i-motif and G-quadruplex (**Figure S5**). These results indicated that **a9** had good selectivity and stability to *c-myc* promoter i-motif and G-quadruplex structures over other gene promoter secondary structures.

Bisacridine derivatives inhibited carcinoma cells proliferation. In order to investigate the anti-tumor activity of the derivatives, we employed MTT assay to evaluate the anti-proliferative activity of our bisacridine derivatives on various human cancer cell lines, such as human melanoma cell line A375, human squamous cervical cancer cell line Hela, human lung adenocarcinoma cell line A549, human bone osteosarcoma epithelial cell line U2OS, human colon cancer cell line HCT116, human cervical cancer cell line SiHa, human hepatocellular carcinoma cell line HuH7. The cytotoxicity of the bisacridine derivatives **a5-28** was determined with their IC_{50} values as shown in **Table 3**. Most of the bisacridine derivatives showed diverse cytotoxicity against various tumor cells. Generally, their activity of inhibiting tumor cell growth was well consistent with their ability of binding to and stabilizing G-quadruplex and i-motif structures. The compounds interacted with both G-quadruplex and i-motif such as **a6-10**, showed potent inhibition to proliferation of tumor cells. **a25-26** exhibited strong stabilizing ability and binding affinity to *c-myc* promoter G-quadruplex and i-motif, however with low cytotoxicity. These two

compounds with relatively high molecular weights, are substituted with easily protonated anime side chains, which could possibly affect their membrane permeability. Indeed, our cell uptake assays (**Figure S7**) showed that cellular uptakes of **a25-26** were much lower than those of compound **a9** and **a11**. Based on above results, **a9** could stabilize *c-myc* promoter G-quadruplex/i-motif with high ΔT_m values, bind the G-quadruplex/i-motif with submicromolar binding constants, and exhibit strong inhibitory effects on the proliferation of tumor cells, and therefore was selected as a promising compound for our further investigation.

Table 3. IC_{50} values of bisacridine derivatives **a5-28** against different cell lines as determined by using MTT assay

Comp.	IC_{50} (μM)						
	A375	Hela	A549	U2OS	HCT116	SiHa	HuH7
a5	6.85	13.81	9.79	5.48	11.09	11.96	19.96
a6	0.13	0.85	0.52	0.44	2.47	0.37	0.27
a7	0.23	0.37	1.16	2.04	1.95	0.49	0.19
a8	0.12	0.34	0.35	0.13	0.19	2.51	0.80
a9	0.28	0.45	0.18	0.31	0.15	1.22	0.16
a10	0.43	0.27	0.28	0.38	0.69	2.00	0.19
a11	1.75	1.36	2.26	1.23	2.12	0.56	1.95
a12	1.88	0.32	0.81	2.16	0.86	2.77	2.14
a13	0.22	0.24	1.14	0.33	0.51	2.26	0.87
a14	2.48	1.36	1.71	2.94	6.25	3.82	6.2

a15	2.05	2.62	1.73	1.60	3.51	3.06	5.56
a16	1.92	1.47	0.47	0.55	2.06	3.70	2.68
a17	0.92	1.36	0.32	0.79	0.91	2.44	3.29
a18	0.51	0.66	0.72	1.33	0.95	1.66	2.81
a19	1.83	1.65	0.83	1.42	1.68	2.52	3.67

Regulation of *c-myc* transcription through interaction with its promoter G-quadruplex and i-motif. As mentioned above, **a9** appeared to be a potent binding ligand to both G-quadruplex and i-motif. **a11** binding to and inducing the formation of *c-myc* G-quadruplex only without significant effect on i-motif was used for comparison. In order to investigate and compare effects of these derivatives on *c-myc* transcription, several experiments were performed, including dual-luciferase reporter assay, reverse transcription-polymerase chain reaction (RT-PCR), and Western blot.

Dual-luciferase reporter assay was performed with a psicheck2 plasmid carrying the *c-myc* promoter in front of the *Renilla Firefly* luciferase gene. After transfection, SiHa cells were incubated with the bisacridine derivatives at concentration of about 1/3 of IC_{50} value for 48 hours. As shown in **Figure S8A**, **a9** could more significantly decrease the ratio of *Renilla*/*Firefly* luciferase activity than **a11**. It should be noted that some other compounds binding to G-quadruplex only did not show good activity in dual-luciferase reporter assay either, which is possibly due to complicated regulatory mechanisms of cells. To identify whether this inhibitory activity was due to its interaction with G-quadruplex/i-motif, we further constructed plasmid

carrying the mutant and deleted *c-myc* promoter, which could not form G-quadruplex/i-motif structures and had no NHE III_1 G/C-rich DNA sequence, respectively. Upon treatment with increasing concentration of **a9**, dose-dependent decrease of the ratio of *Renilla*/*Firefly* luciferase activity was observed for wild-type plasmid but not for mutant or deleted plasmid (**Figure S8B**), suggesting that **a9** presumably interacted with *c-myc* G/C-rich DNA sequence to affect *Renilla*/*Firefly* luciferase activity.

Reverse transcription-polymerase chain reaction (RT-PCR) was performed to determine effect of **a9** on regulation of *c-myc* gene transcription in cells. **a11** binding to and inducing *c-myc* G-quadruplex formation only was again used for comparison. SiHa cells were incubated with **a9** and **a11** at increasing concentration of 0, 1.25, 2.5, 5.0 μM for 3 hours. As shown in **Figure 4A**, the treatment of the cells with **a9** and **a11** both caused reductions of *c-myc* mRNA levels in dose-dependent manners in SiHa cells, and **a9** obviously had more significant effect on transcriptional regulation. The levels of *c-myc* mRNA were reduced for up to 40.1%, 76.9% and 92.7%, relative to a β-actin control with treatment of 1.25, 2.5 and 5.0 μM **a9**, while the same concentrations of **a11** reduced the mRNA levels for only 32.6%, 55.8% and 79.8%, respectively. Since *c-myc* mRNA also contains G-quadruplex on its 5'UTR, it is necessary to know whether **a9** could affect stability of *c-myc* mRNA. Actinomycin D is a known antibiotic inhibiting mRNA synthesis.[46] Our incubation of SiHa cells with Actinomycin D in the presence and absence of **a9** showed almost the same degradation velocity of *c-myc* mRNA (**Figure S9**), indicating that **a9** had no significant effect on stability of *c-myc* mRNA.

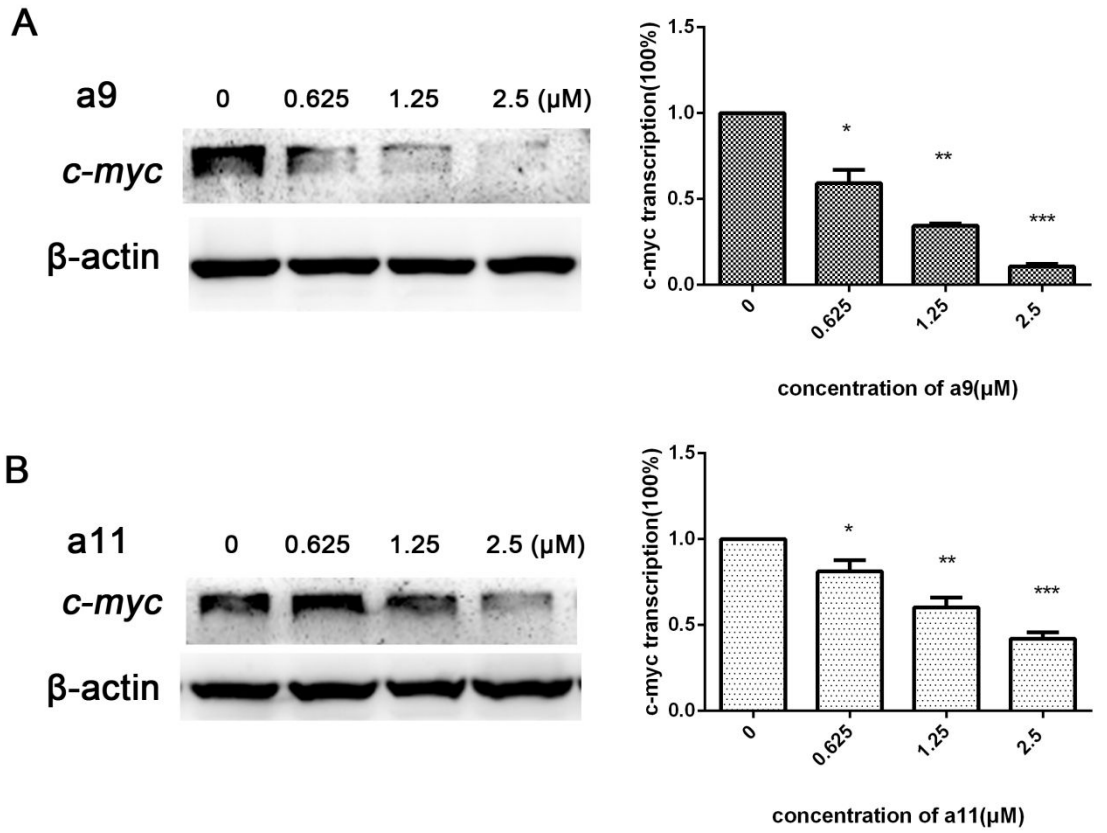

Figure 4. Effect of **a9** or **a11** on *c-myc* transcription and expression after 24 h treatment of SiHa cells. Left, Western blot was used to determine the expression levels of C-MYC in SiHa cells treated with increasing concentrations of **a9** (A) or **a11** (B) (0, 0.625, 1.25, and 2.5 μM) for 24 h. β-actin was used as an intracellular house-keeping protein. Right, qRT-PCR was used to determine *c-myc* transcription in SiHa cells treated with increasing concentrations of **a9** (A) or **a11** (B) (0, 0.625, 1.25, and 2.5 μM) for 24 h. β-actin was used as an internal control. The experiments were repeated for three times: *, $P < 0.05$; **, $P < 0.01$; ***, $P < 0.001$.

To further identify whether this transcriptional inhibition happened through interaction of **a9** with *c-myc* promoter G-quadruplex/i-motif forming sequence, Raji and CA46 cells (Two Burkitt's lymphoma cell lines) were comparatively incubated with **a9**, which has been regarded as a

necessary experiment to determine whether a ligand is targeting *c-myc* promoter G-quadruplex/i-motif sequence in cells.[47-49] As reported previously, *c-myc* promoter G-quadruplex/i-motif forming sequence could exist in the fragment of nontranslocated chromosome in Raji cells but not in translocated chromosome in CA46 cells. If the mechanism of *c-myc* transcriptional modulation is mediated through its promoter G-quadruplex/i-motif sequence, a preferential change should be evident with a functional MYC under the control (**Figure S10A**).[50-51] As shown in **Figure S10B**, **a9** produced a dose-dependent transcriptional down-regulation of *c-myc* in Raji cells. In comparison, treatment of CA46 cells with increasing concentration of **a9** did not cause a reduction of *c-myc* mRNA in a dose-dependent manner (**Figure S10C**). These results indicated that **a9** could directly target *c-myc* promoter G-quadruplex/i-motif forming sequence in cells.

Western blot was also carried out to measure C-MYC protein expression levels, as shown in **Figure 4B**. The expression levels of C-MYC were reduced for up to 39.8, 73.9 and 92.2% relative to a GAPDH control upon treatment with 1.25, 2.5 and 5.0 μM **a9**, respectively. In comparison, upon treatment with the same concentrations of **a11**, C-MYC protein levels were reduced for only 25.3, 42.2 and 62.3%, respectively. These results showed that upon incubation with increasing concentrations of compound **a9** and **a11**, the expression levels of C-MYC both decreased in dose-dependent manners. **a9** as a dual G-quadruplex/i-motif binder, could down-regulate *c-myc* gene expression more effectively than **a11** that interacted with G-quadruplex only.

Effect of compound a9 on cancer cells apoptosis and cycle arrest. Since *c-myc* is a key

oncogene related to several cellular events, suppression of oncogenic *c-myc* transcription and expression by small molecules has significant anti-tumor effect on various types of tumor cells. Our above studies indicated that **a9** could bind to both G-quadruplex and i-motif of *c-myc* promoter resulting in down-regulation of *c-myc* transcription and translation. Therefore, we further studied its anti-tumor activity with other biophysical and biochemical methods. As mentioned above, **a9** could inhibit SiHa cells short-term proliferation with IC_{50} value of 1.22 μM. Its inhibitory effect on cell proliferation was further investigated through colony formation assay and transwell assay to study its inhibition of tumor cells long-term proliferation and invasion, respectively. As shown in **Figure S11A**, upon incubation with **a9**, colony formation obviously decreased, suggesting inhibition of cell proliferation, which was consistent with our MTT results. For comparison, we used Pyridostatin (PDS) as a well-known G-quadruplex stabilizing ligand[52] to study and compare effects of G-quadruplex ligands on cells proliferation, and **a9** showed obviously more significant effect on SiHa cells colony formation. Then, SiHa cells were incubated with 0.5 μM **a9** for 24 hours, and the cells migration was reduced for approximately 85% as shown in **Figure S11B**, indicating that **a9** could inhibit SiHa cells invasion. The above results suggested that **a9** could inhibit proliferation and invasion of cancer cells, which could be due to its repression of *c-myc* transcription.

It has been previously reported that decreased expression of *c-myc* could induce cellular apoptosis and cell cycle arrest of proliferating cancer cells.[53-54] Therefore, we investigated whether **a9** could induce cellular apoptosis and cell cycle arrest of SiHa cells through down-regulation of *c-myc* transcription. SiHa cells treated with **a9** were analyzed by using flow cytometry. As shown

in **Figure 5**, G2/M phase cell cycle arrest was significant for SiHa cells treated with **a9** for 24 hours, compared with the control group. The cells were arrested at G2/M phase for up to 56.9% upon treatment with 0.6 μM **a9**. Besides, A sub G0 peak was observed upon treatment with 0.6 μM of **a9**. SiHa cells treated with or without **a9** were examined for apoptosis by using PI and annexin V staining. As shown in **Figure 6A-B**, upon incubation of SiHa cells with **a9** at increasing concentration of 0, 0.6, 1.2, and 2.4 μM for 24 hours, both early and late cell apoptosis were induced. The percentages of early apoptosis cells were 0.3%, 18.1%, 43.2%, and 55.4%, while the percentages of late apoptosis cells were 0.4%, 3.8%, 18.7%, and 27.5%, respectively. Our results indicated that **a9** could induce SiHa cell cycle arrest at G2/M phase and apoptosis, possibly through repression of *c-myc* transcription.

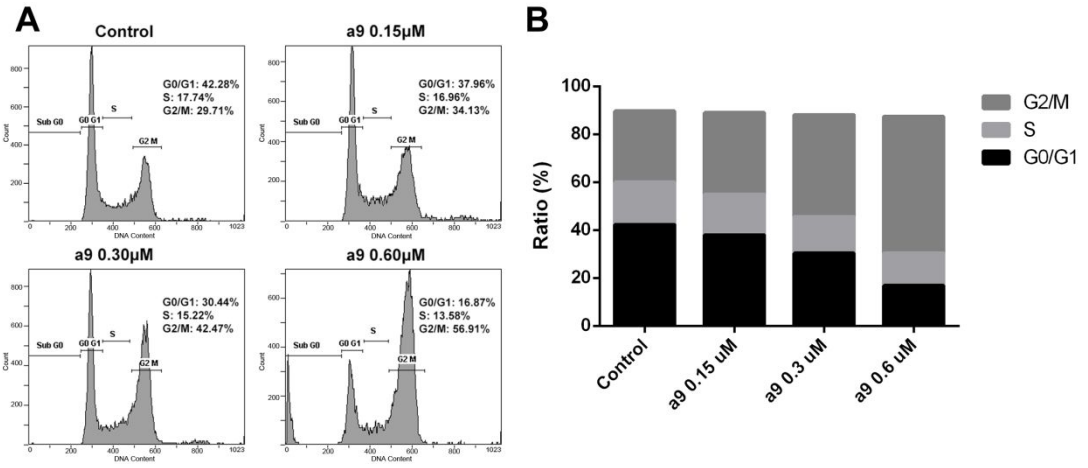

Figure 5. Cell cycle arrest of SiHa cells with or without treatment of **a9**. (A) Cell cycle analysis after 24 h treatment with different concentrations of **a9**, followed with propidium iodide (PI) staining and EXPO32 ADC software analysis. (B) Percentage of cells in different phases of the cell cycle. All the experiments were repeated for three times.

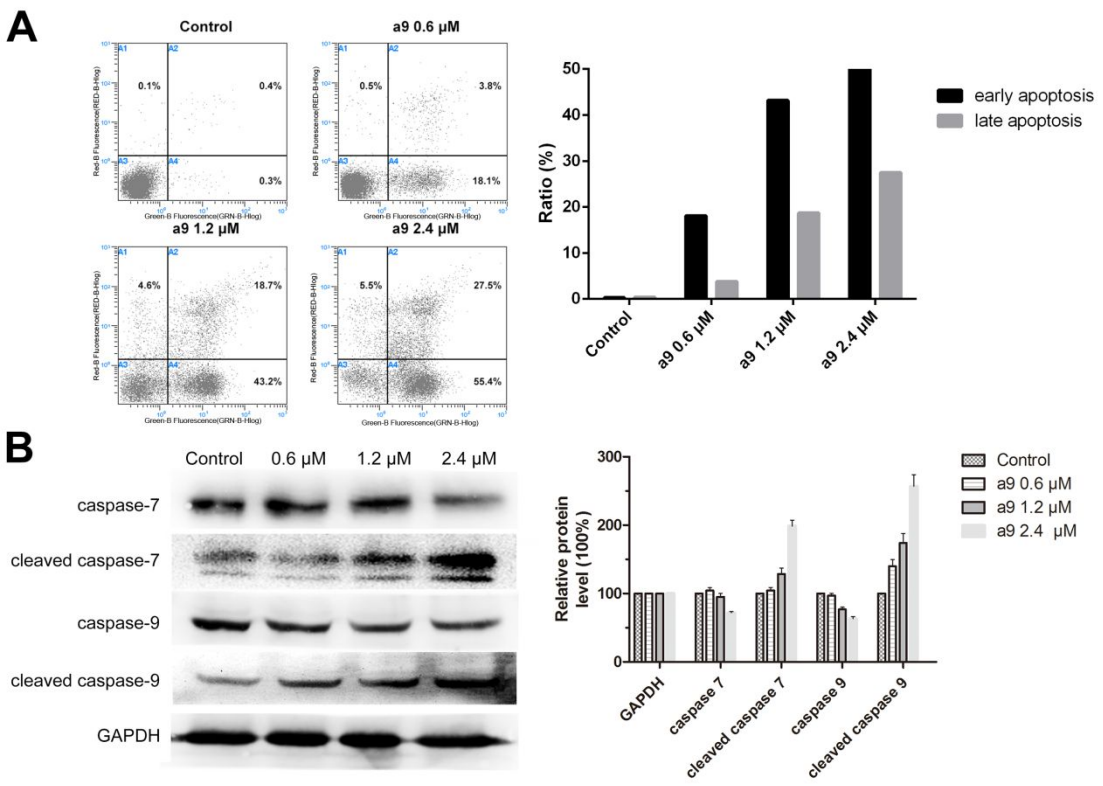

Figure 6. Inhibition of cell proliferation by inducing cell apoptosis. SiHa cells were treated with increasing concentrations of **a9**. (A) Cell apoptosis was measured by using Annexin - FITC/PI double-staining flow cytometry. Quantitative analysis of the percentage of cells in each cell cycle was performed by using EXPO32 ADC analysis software. (B) Analysis of the levels for the apoptosis-related proteins caspase-7, cleaved caspase-7, caspase-9, and cleaved caspase-9 was performed through Western blot. The protein bands were quantified by using Quantity One. All these experiments were repeated for three times.

Since activation of caspases is an important process during cell apoptosis, the detection of apoptosis markers such as caspase 7, cleaved caspase 7, caspase 9 and cleaved caspase 9 in SiHa

cells upon treatment with **a9** was carried out using Western blot. As shown in **Figure 6B**, upon treatment with increasing concentration of **a9**, the levels of caspase 7 and caspase 9 decreased in dose-dependent manners. On the contrary, cleaved caspase 7 and cleaved caspase 9 showed dose-dependent increase upon treatment with **a9**, suggesting that **a9** induced apoptosis possibly through decreasing the levels of active caspases 7 and 9 while activating cleaved caspase 7 and cleaved caspase 9 in cancer cells.

Besides, we studied and compared the effects of **a9** and PDS on cells proliferation, apoptosis and cell cycle distribution for Raji and CA46 cells. PDS has been shown to silence a series of oncogenes including *c-myc* and SRC, which showed inhibition on both Raji and CA46 cells in the present study. In contrast, **a9** inhibited only Raji cells proliferation, and induced Raji cells apoptosis and cycle arrest at G2/M phase, without significant effect on CA46 cells (**Table S5**, **Figure S12**, **Figure S13**). These results further indicated that **a9** repressed tumor cells growth through down-regulation of *c-myc* transcription.

Compound a9 inhibited tumor growth in a SiHa cervical xenograft. Since above results showed that **a9** could down-regulate *c-myc* gene transcription and inhibit tumor cells growth, its anti-tumor activity was further evaluated against a human cervical cancer xenograft (SiHa) in athymic nude mice, as shown in **Figure 7A-C**. An experimental group of six tumor-bearing mice was treated with **a9** once two days at a dosage of 15 mg/kg for 18 days. No significant change in body weight was observed during the treatment with **a9** (**Figure 7A**). The negative control group, which was treated with saline only, had an average tumor volume of 750 mm^3 after 18 days. In contrast, the tumor-bearing mice treated with **a9** had an average tumor volume of 450 mm^3. The

tumor weight in the presence of **a9** reduced around 41.6% to a final weight of 0.55g (**Figure 7B**). The positive control group was treated once two days with cisplatin at a dosage of 0.2 mg/kg for 18 days, with average tumor volume reduced to 200 mm^3 and average tumor weight reduced to 0.18g. These results suggested that **a9** had good anti-tumor activity on the SiHa xenografted mice. The effect of compound **a9** on various organs was also assessed as shown in **Figure 7D**, and no significant change was observed. This indicated that **a9** could have high selectivity to tumor cells without significant toxicity to normal body in comparison with cisplatin.

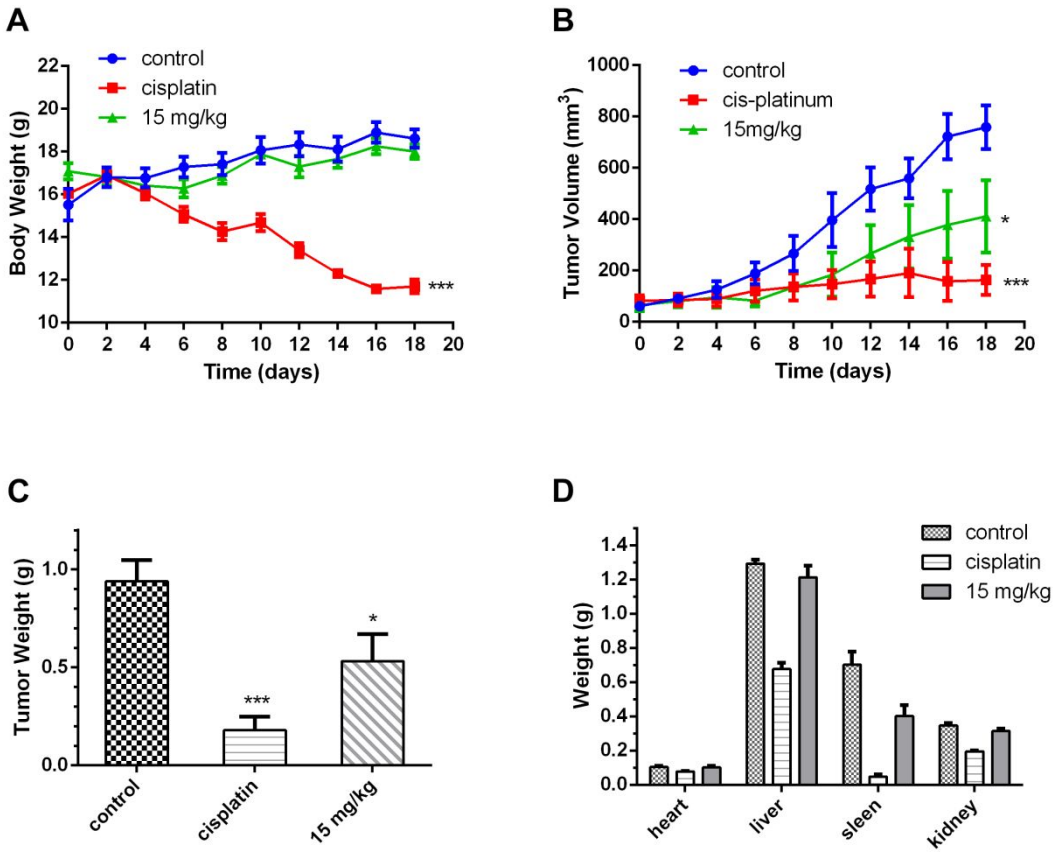

Figure 7. Evaluation of the tumor growth inhibition by **a9** in a SiHa xenograft model. (A) The body weights were measured and recorded every two days. (B) Tumor volumes of the mice in

each group during the observation period. The volume (mm^3) = length (mm) × width $(mm)^2/2$. (C) The average weights of the excised tumors from each group. (D) Organs weights of the mice in each group at the end of the observation period.

Molecular docking studies for the binding of compound a9 to *c-myc* promoter G-quadruplex and i-motif. Molecular docking studies were performed to understand possible interactions of **a9** with *c-myc* promoter G-quadruplex and i-motif structures by using the MOE program. **a9** was docked to *c-myc* promoter G-quadruplex (PDB ID: 2l7v) structure. However, either NMR or X-ray crystallographic structure of *c-myc* promoter i-motif is not available in literature, and therefore telomeric i-motif DNA (PDB ID: 1eln) was used as a model structure for analyzing possible binding interactions of **a9** to i-motif. As shown in **Figure 8A**, our docking result for interaction of **a9** with *c-myc* promoter G-quadruplex showed that one acridine ring could stack on the external 5′-terminal G-quartet through a π-π stacking interaction, and another acridine backbone could possibly lay on the DNA groove space. **a9** should be positively charged in physiological condition, which could interact with negatively charged phosphate diester backbone of *c-myc* promoter G-quadruplex through electrostatic interactions. The amine linker could form two important H-bonds with the backbone of *c-myc* promoter G-quadruplex in distances of 3.3Å and 3.5Å. Our docking result for interaction of **a9** with *c-myc* promoter i-motif was shown in **Figure 8B**. Our docking result showed that both acridine rings of **a9** could interact with i-motif through π-π stacking interactions. Similar to the binding interaction of **a9** with *c-myc* promoter G-quadruplex, **a9** could interact with i-motif through electrostatic interactions and H-bonds in

distances of 3.2Å. Our UV-titration data showed that the absorption peak of **a9** shifted toward a longer wavelength in the present of G-quadruplex or i-motif, indicating the π-π stacking interactions between **a9** and G-quadruplex or i-motif (**Figure S14**). This result was in accordance with the docking study. These results further reinforced our design to have acridine dimer for interacting with both G-quadruplex and i-motif.

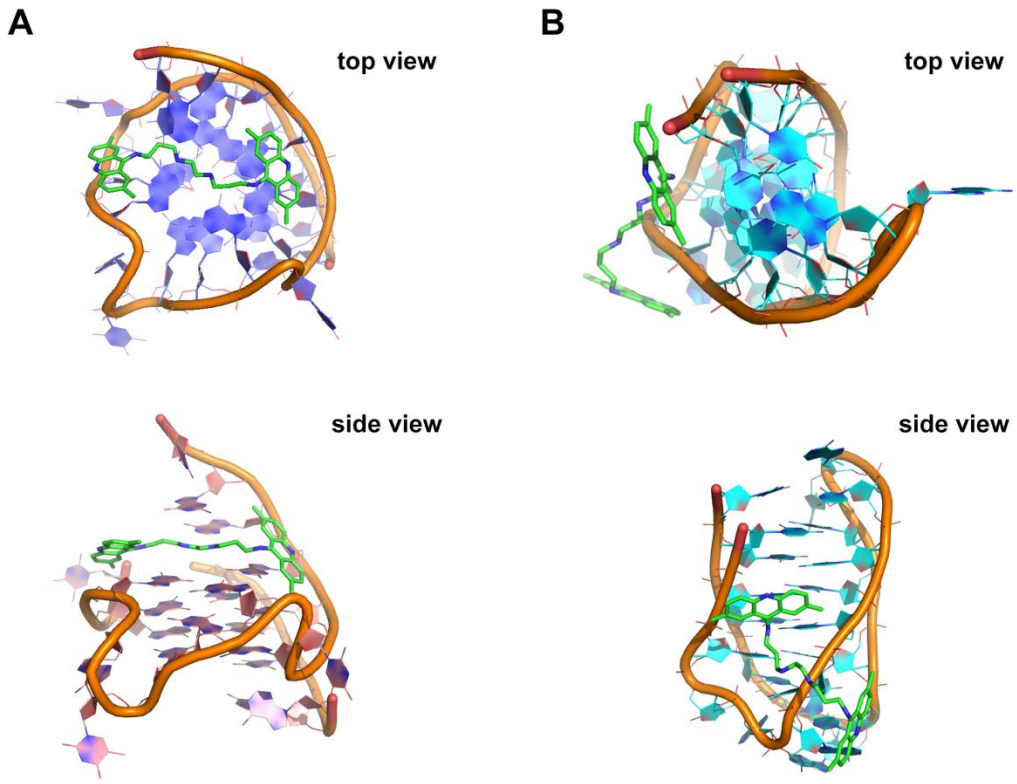

Figure 8. Hypothetical binding mode of **a9** to *c-myc* promoter DNA secondary structures. A. top views for binding of **a9** to the 5′ end of *c-myc* promoter G-quadruplex (PDB code 2L7V) and side views. B. top views for binding of **a9** to a model tetrameric i-motif (PDB ID: 1YBL) and side views.

Conclusion

It should be noted that previous efforts have been largely focused on study of G-quadruplex binding ligands, while i-motif binding ligands have been much less studied. In the present study, we explored a new strategy of targeting both G-quadruplex and i-motif on *c-myc* oncogene promoter for transcriptional regulation through syntheses and evaluation of disubstituted bisacridine derivatives. FRET, NMR, SPR, ITC and CD experiments were carried out to study the effects of different disubstituted derivatives with various chain linkers on binding to and stabilization of *c-myc* promoter G-quadruplex/i-motif. Our FRET and SPR results showed that our bisacridine derivatives with substitutive groups had generally weak binding and stability to duplex DNA, indicating their insignificant intercalating effect compared with their binding affinity to *c-myc* promoter G-quadruplex/i-motif. Compound **a9** was found to be a potent dual G-quadruplex/i-motif binder and selected for further biological evaluation. **a9** could down-regulate *c-myc* gene transcription and expression, possibly through stabilization of *c-myc* promoter G-quadruplex/i-motif. Our cellular experiments showed that **a9** exhibited anti-proliferative effect on cancer cells by inducing cell apoptosis and cycle arrest. Its anti-proliferative effect was further evaluated with a cervical cancer xenograft model, indicating its high selectivity to SiHa cancer cells.

The population of G−quadruplexes has been found to be maximal in S phase of cell cycle by using antibody staining, consistent with cellular replication dependent formation of G−quadruplexes. The formation of i-motifs varied over the cell cycle with the highest level

occurred in late G1 phase, which is characterized by high levels of transcription and cellular growth. G-quadruplex and i-motif of *c-myc* oncogene promoter may serve as dual regulating system to securely lock down oncogene transcription and expression. Our present study showed that **a9** as a dual G-quadruplex/i-motif binder, could down-regulate *c-myc* gene transcription and induce cell apoptosis more effectively than **a11** that interacted with G-quadruplex only. **a9** as a dual G-quadruplex/i-motif binder, could be effective on both oncogene replication and transcription, while **a11** could be effective mainly on oncogene replication stage. **a9** could become a promising lead compound for further development for cancer treatment targeting both *c-myc* promoter G-quadruplex and i-motif with improved potency and selectivity. Our present results increased our understanding of gene regulation system, which shed light on development of improved anticancer drugs.

EXPERIMENTAL SECTION

General Methods for Syntheses. All chemicals were purchased from commercial sources used as starting materials, which were analytical grade without further purification unless otherwise specified. All synthesized compounds were confirmed by using ^{1}H, ^{13}C NMR spectra and HRMS spectrometry. ^{1}H and ^{13}C NMR spectra were recorded using TMS as the internal standard in DMSO-d_6, CD_3OD, or $CDCl_3$ with a Bruker BioSpin GmbH spectrometer at 400 and 100 MHz, respectively. High resolution mass spectra (HRMS) were recorded on Shimadzu LCMS-IT-TOF of MAT95XP mass spectrometer (Thermo Fisher Scientific, USA). The purity of the synthesized compound was confirmed to be higher than 95% by using analytical HPLC performed with a dual

pump Shimadzu LC-20 AB system equipped with an Ultimate XB-C18 column (4.6 mm × 250 mm, 5 μm), eluting with methanol-water (10:90 to 60:40) containing 0.05% TFA at a flow rate of 0.5 mL/min.

The intermediates were prepared following the process shown in **Scheme 1**.

Synthesis of 5-substituted-2-(4-substituted-phenylamino)benzoic acid (**2**)

To a solution of 2-amino-5-substituted-benzoic acid (**1**, 19.87 mmol) in anhydrous dimethylformamide (50 mL), were added 1-bromo-4-substituted-benzene (59.6 mmol, 3 equiv), anhydrous potassium carbonate (4.11g, 29.8 mmol), copper powder (300 mg), copper iodide (100 mg). The mixture was stirred and heated under reflux and nitrogen atmosphere, monitored by using TLC. After cooling down, the mixture was poured into ice water and stirred, with pH adjusted to 3-4. Ethyl acetate (100 mL) was added and stirred for another 10 mins, filtered, and the residue was extracted with ethyl acetate (3×50 mL). The combined organic layer was washed with diluted hydrochloric acid, and then brine for three times, dried over anhydrous sodium sulfate, filtered, and concentrated under reduced pressure to give crude compound **2**, which was used for the next step without purification.

Synthesis of 2-substituted-7-substituted-acridin-9(10H)-one (**3**)

To a 100 mL round bottom flask containing residue **2** (4.0 g), was added 10 mL concentrated sulfuric acid. The mixture was stirred at 100 ^{o}C under nitrogen atmosphere, monitored by using TLC. After cooling down, the reaction mixture was poured into ice water and stirred, filtered, and the solid was washed with saturated sodium bicarbonate, dried to give crude compound **3**, which

was used for the next step without purification.

Synthesis of 9-chloro-2-substituted-7-substituted-acridine (**4**)

To a 100 mL round bottom flask containing residue **3** (3.0 g), was added $POCl_3$ (10 mL) dropwise, followed with DMF (0.1 mL) at 0-5 ^oC. The reaction mixture was stirred for 30 mins, and then heated to 100 ^oC slowly with stirring, which was monitored until reaction completed by using TLC. After cooling down, the solvent was removed, and the residue was poured into ice water with stirring. Ethyl acetate (50 mL) was added, and pH was adjusted to 9-10 with sodium bicarbonate. The resulting solution was filtered, and the water phase was extracted with ethyl acetate (20 mL × 3). The combined organic layer was washed with brine for three times, dried over anhydrous sodium sulfate, filtered, and then concentrated under reduced pressure. The residue was purified by using chromatograph on silica gel with petroleum ether / ethyl acetate (10/1 - 2/1) to give the desire intermediate **4**, with an overall yield of 20-30 % for three steps.

9-chloro-2,7-dimethylacridine (**4a**), yellow solid, yield 30%. ^1H NMR (400 MHz, $CDCl_3$) δ 8.15 (s, 2H), 8.10 (d, J = 8.9 Hz, 2H), 7.61 (dd, J = 8.9, 1.8 Hz, 2H), 2.61 (s, 6H). ESI-MS (m/z) 242 $[M + H]^+$.

9-chloro-2-methylacridine (**4b**), yellow solid, yield 20%. ^1H NMR (400 MHz, $CDCl_3$) δ 8.42 (dd, J = 8.7, 0.5 Hz, 1H), 8.27 – 8.16 (m, 2H), 8.13 (d, J = 8.9 Hz, 1H), 7.78 (ddd, J = 8.7, 7.9, 4.7 Hz, 1H), 7.69 – 7.57 (m, 2H), 2.63 (s, 3H). ESI-MS (m/z) 228 $[M + H]^+$.

9-chloroacridine (**4c**), yellow solid, yield 24%. ^1H NMR (400 MHz, $CDCl_3$) δ 8.11 (dd, J = 7.5, 1.4 Hz, 2H), 8.03 (dd, J = 7.5, 1.6 Hz, 2H), 7.75-7.71 (m, 2H), 7.61-7.57 (m, 2H). ESI-MS (m/z)

228 $[M + H]^+$.

Synthesis of 2-((4-carboxyphenyl)amino)-5-methylbenzoic acid (**6**)

Based on the procedure for preparation of compound **2**, with bromobenzene replaced by 4-bromobenzoic acid, a crude intermediate **6** was obtained and used for the next step without purification.

Synthesis of ethyl 7-methyl-9-oxo-9,10-dihydroacridine-2-carboxylate (**7**)

To a 100 mL round bottom flask containing residue **6** (4.0 g, crude), was added 10 mL concentrated sulfuric acid. The reaction mixture was stirred at 120 ^oC under nitrogen atmosphere, and monitored by using TLC. After cooling down, ethanol (50 mL) was added dropwise at 0 ^oC. The mixture was heated under reflux under nitrogen atmosphere for 2 hours. After cooling down, the reaction mixture was poured into ice water with stirring, filtered, and the solid was washed with saturated sodium bicarbonate, dried and purified by using chromatograph on silica gel with DCM/MeOH (80/1-10/1) to give **7** as a yellow solid with an overall yield of 30% for three steps. ^1H NMR (400 MHz, DMSO) δ 11.98 (s, 1H), 8.81 (d, J = 1.8 Hz, 1H), 8.16 (dd, J = 8.8, 2.0 Hz, 1H), 8.02 (s, 1H), 7.63 – 7.52 (m, 2H), 7.47 (d, J = 8.4 Hz, 1H), 4.35 (q, J = 7.1 Hz, 2H), 2.43 (s, 3H), 1.37 (t, J = 7.1 Hz, 3H). ^{13}C NMR (101 MHz, DMSO) δ 176.49, 165.28, 143.45, 138.77, 135.38, 132.71, 131.23, 128.61, 125.17, 121.75, 120.77, 119.43, 117.70, 117.60, 60.59, 20.53, 14.23. ESI-MS (m/z) 282 $[M + H]^+$.

Synthesis of 7-methyl-9-oxo-9,10-dihydroacridine-2-carboxylic acid (**8**)

To a solution of **7** (2.0 g, 7.12 mmol) in MeOH (30 mL), was added 5 mL 10% sodium hydroxide solution. The mixture was stirred at 60 °C and monitored with TLC until completion of reaction. After cooling down, the mixture was concentrated, and 20 mL ice water was added. The mixture was stirred with pH adjusted to 5-6, filtered and washed with H_2O, dried to give intermediate **8** as a crude solid, which was used for the next step without purification.

Synthesis of 9-chloro-*N*-(3-(dimethylamino)propyl)-7-methylacridine-2-carboxamide (**9**)

To a 100 mL round bottom flask containing intermediate **8** (400 mg, 1.58 mmol), was added 5 mL $SOCl_2$ dropwise followed with 3 drops of DMF at 0-5 °C. The reaction mixture was heated to 80 °C slowly and reacted for 2 hours. After cooling down to room temperature, the solvent was evaporated and the residue was dissolved in TCM (10 mL). The reaction mixture was cooled to 0 °C, and then N^1,N^1-dimethylpropane-1,3-diamine (322 mg, 3.16 mmol) and TEA (638 mg, 6.32 mmol) were added with stirring for 1h. The reaction mixture was quenched and poured into ice water with stirring, and filtered. The water layer was extracted with DCM (10 mL × 3), and combined organic layers were washed with brine, dried over anhydrous sodium sulfate, filtered and concentrated under reduced pressure, and purified by using chromatograph on silica gel with DCM/MeOH (20/1-5/1, contained 1 % $NH_3 \cdot H_2O$) to give **9** as a yellow solid, with an overall yield of 33% for three steps. ^{1}H NMR (400 MHz, DMSO) δ 9.05 (t, J = 5.4 Hz, 1H), 8.87 (d, J = 1.0 Hz, 1H), 8.26 (dd, J = 9.1, 1.7 Hz, 1H), 8.21 (d, J = 9.0 Hz, 1H), 8.14 (s, 1H), 8.11 (d, J = 8.9 Hz, 1H), 7.80 (dd, J = 8.9, 1.4 Hz, 1H), 3.41 (q, J = 12.7, 6.7 Hz, 2H), 2.61 (s, 3H), 2.49 (t, J = 7.3 Hz, 2H),

2.31 (s, 6H), 1.86 – 1.74 (m, 2H). ^{13}C NMR (101 MHz, DMSO) δ 165.78, 148.71, 148.62, 140.52, 138.56, 135.00, 133.32, 130.20, 129.84, 129.02, 124.39, 124.18, 123.18, 122.61, 56.99, 45.05, 38.29, 26.92, 22.13. ESI-MS (m/z) 356 $[M + H]^+$.

Synthesis of methyl 9-chloro-7-methylacridine-2-carboxylate (**10**)

Based on the procedure for preparation of **9**, with N^1,N^1-dimethylpropane-1,3-diamine replaced by MeOH, a crude intermediate **10** was obtained and purified by using chromatograph on silica gel with petroleum ether / ethyl acetate (5/1 - 1/1) to give **10** as a yellow solid, with an overall yield of 53% for three steps. ^{1}H NMR (400 MHz, $CDCl_3$) δ 9.20 (s, 1H), 8.33 (d, J = 9.1 Hz, 1H), 8.23 (d, J = 9.0 Hz, 1H), 8.19 (s, 1H), 8.14 (d, J = 8.8 Hz, 1H), 7.71 (d, J = 8.9 Hz, 1H), 4.04 (s, 3H), 2.64 (s, 3H). ESI-MS (m/z) 286 $[M + H]^+$.

General procedure for preparation of acridine derivatives **a5-a28**

To a solution of intermediate **4**, **9**, or **10** (0.42 mmol, 2.05 equiv) in 2 mL phenol, was added various alkylamine (NH_2-L-NH_2, 0.2 mmol). The mixture was stirred at 100 °C under nitrogen atmosphere, which was monitored by using TCL. After cooling down, ethyl acetate (20 mL) was added with stirring at 0 °C, and then 15 mL ice cold 20% NaOH was added dropwise followed with stirring for 20 mins. The solution was extracted with ethyl acetate (5 mL × 3), and the combined organic phase was washed with 5% NaOH, then brine, and dried over anhydrous sodium sulfate. The solution was filtered, concentrated under reduced pressure, and purified by using chromatograph on silica gel with DCM/MeOH (10/1-5/1, containing 1% $NH_3 \cdot H_2O$) to give

a5-a28.

N^1-(acridin-9-yl)-N^2-(2-(acridin-9-ylamino)ethyl)ethane-1,2-diamine (**a5**). Yellow solid, yield 88%. ^{1}H NMR (400 MHz, $CDCl_3$) δ 8.13 (d, *J* = 8.6 Hz, 2H), 8.06 (d, *J* = 8.0 Hz, 2H), 7.66 – 7.60 (m, 2H), 7.31 – 7.22 (m, 2H), 3.93 (t, *J* = 5.0 Hz, 2H), 3.06 (t, *J* = 5.0 Hz, 2H). ^{13}C NMR (101 MHz, $CDCl_3$) δ 151.69, 148.63, 130.11, 129.52, 123.07, 116.92, 115.85, 49.75, 49.61. Purity was determined to be 97.2% by using HPLC. HRMS (ESI; m/z). Calcd for C30H27N5, $[M + H]^+$, 458.2339; found:458.2332.

N^1-(2,7-dimethylacridin-9-yl)-N^3-(3-((2,7-dimethylacridin-9-yl)amino)propyl)-N^3-methylpropane-1,3-diamine (**a6**). Yellow solid, yield 60%. ^{1}H NMR (400 MHz, $CDCl_3$) δ 7.92 (d, *J* = 8.8 Hz, 2H), 7.73 (s, 2H), 7.39 (dd, *J* = 8.8, 1.3 Hz, 2H), 3.82 (t, *J* = 6.3 Hz, 2H), 2.60 (t, *J* = 6.3 Hz, 2H), 2.39 (s, 6H), 2.38 (s,3H), 1.98 – 1.83 (m, 2H). ^{13}C NMR (101 MHz, $CDCl_3$) δ 149.82, 147.76, 132.31, 131.94, 129.39, 121.14, 116.93, 56.91, 50.34, 42.64, 28.30, 21.92. Purity was determined to be 95.7% by using HPLC. HRMS (ESI; m/z). Calcd for C37H41N5, $[M + H]^+$, 556.3361; found: 556.3382.

N^1-methyl-N^3-(2-methylacridin-9-yl)-N^1-(3-((2-methylacridin-9-yl)amino)propyl)propane-1,3-diamine (**a7**). Yellow solid, yield 53%. ^{1}H NMR (400 MHz, $CDCl_3$) δ 7.99 (d, *J* = 8.7 Hz, 4H), 7.91 (d, *J* = 8.7 Hz, 2H), 7.71 (s, 2H), 7.53 (t, *J* = 7.6 Hz, 2H), 7.39 (d, *J* = 8.7 Hz, 2H), 7.15 (t, *J* = 7.6 Hz, 2H), 3.86 (t, *J* = 6.2 Hz, 4H), 2.60 (t, *J* = 6.1 Hz, 4H), 2.38 (s, 9H), 1.97 – 1.84 (m, 4H).

^{13}C NMR (101 MHz, $CDCl_3$) δ 150.78, 148.80, 147.69, 132.40, 132.33, 129.44, 129.18, 129.07, 128.95, 123.20, 122.41, 121.05, 116.47, 56.88, 50.36, 42.64, 28.14, 21.94. Purity was determined to be 98.4% by using HPLC. HRMS (ESI; m/z). Calcd for C35H37N5, $[M + H]^+$, 528.3141; found: 528.3147.

N^1-(acridin-9-yl)-N^3-(3-(acridin-9-ylamino)propyl)-N^3-methylpropane-1,3-diamine (**a8**). Yellow solid, yield 41%. ^{1}H NMR (400 MHz, $CDCl_3$) δ 7.96 (d, *J* = 8.5 Hz, 4H), 7.91 (d, *J* = 8.7 Hz, 4H), 7.49 (t, *J* = 7.5 Hz, 4H), 7.09 (t, *J* = 7.6 Hz, 4H), 3.77 (t, *J* = 5.7 Hz, 4H), 2.48 (t, *J* = 5.3 Hz, 4H), 2.27 (s, 3H), 1.84 – 1.76 (m, 4H). ^{13}C NMR (101 MHz, $CDCl_3$) δ 151.66, 148.80, 129.86, 128.48, 123.25, 122.29, 116.10, 56.66, 50.18, 42.46, 27.85. Purity was determined to be 97.8% by using HPLC. HRMS (ESI; m/z). Calcd for C33H33N5, $[M + H]^+$, 500.4382; found: 500.4398.

N^1,$N^{1'}$-(ethane-1,2-diyl)bis(N^3-(2,7-dimethylacridin-9-yl)propane-1,3-diamine) (**a9**). Yellow solid, yield 58%. ^{1}H NMR (400 MHz, $CDCl_3$) δ 7.95 (d, *J* = 8.6 Hz, 1H), 7.82 (s, 1H), 7.44 (d, *J* = 8.7 Hz, 1H), 3.85 (t, *J* = 7.5 Hz, 1H), 2.87 (s, 2H), 2.49 (s, 3H), 1.87-1.82 (m, 1H). ^{13}C NMR (101 MHz, $CDCl_3$) δ 150.20, 147.78, 132.20, 132.03, 129.31, 121.40, 116.87, 50.68, 49.75, 48.86, 30.78, 22.11. Purity was determined to be 100% by using HPLC. HRMS (ESI; m/z). Calcd for C38H44N6, $[M + H]^+$, 585.2881; found: 585.2880.

N^1,$N^{1'}$-(ethane-1,2-diyl)bis(N^3-(acridin-9-yl)propane-1,3-diamine) (**a10**). Yellow solid, yield 45%. ^{1}H NMR (400 MHz, CD_3OD_ SPE) δ 8.16 (d, *J* = 8.6 Hz, 1H), 7.76 (d, *J* = 8.7 Hz, 1H),

7.58 (t, *J* = 7.6 Hz, 1H), 7.24 (t, *J* = 7.6 Hz, 1H), 3.86 (t, *J* = 6.4 Hz, 1H), 2.73 – 2.59 (m, 2H), 1.93 – 1.77 (m, 1H). ^{13}C NMR (101 MHz, CD_3OD_SPE) δ 153.06, 147.62, 130.49, 125.89, 123.85, 121.97, 115.33, 70.14, 48.78, 48.45, 29.73. Purity was determined to be 96.2% by using HPLC. HRMS (ESI; m/z). Calcd for C34H36N6, $[M + H]^+$, 529.3151; found: 529.3153.

N,N'-((ethane-1,2-diylbis(oxy))bis(ethane-2,1-diyl))bis(2,7-dimethylacridin-9-amine) (**a11**). Yellow solid, yield 52%. ^{1}H NMR (400 MHz, $CDCl_3$) δ 7.98 (d, *J* = 8.8 Hz, 1H), 7.82 (s, 1H), 7.42 (d, *J* = 8.8 Hz, 1H), 3.84 (t, *J* = 4.8 Hz, 1H), 3.69 (s, 1H), 3.62 (t, *J* = 4.8 Hz, 1H), 2.45 (s, 3H). ^{13}C NMR (101 MHz, $CDCl_3$) δ 149.76, 147.29, 133.22, 132.32, 128.98, 121.04, 118.30, 70.51, 70.36, 50.21, 22.02. Purity was determined to be 95.2% by using HPLC. HRMS (ESI; m/z). Calcd for C36H38N4O2, $[M + H]^+$, 559.3062; found: 559.3060.

N,N'-((ethane-1,2-diylbis(oxy))bis(ethane-2,1-diyl))bis(2-methylacridin-9-amine) (**a12**). Yellow solid, yield 52%. ^{1}H NMR (400 MHz, $CDCl_3$) δ 8.08 (d, *J* = 8.7 Hz, 1H), 7.97 (d, *J* = 8.6 Hz, 1H), 7.87 (d, *J* = 8.8 Hz, 1H), 7.82 (s, 1H), 7.51 (t, *J* = 7.6 Hz, 1H), 7.33 (d, *J* = 8.7 Hz, 1H), 7.22 (t, *J* = 7.6 Hz, 1H), 3.91 (t, *J* = 4.8 Hz, 2H), 3.77 (t, *J* = 4.7 Hz, 2H), 3.75 - 3.73 (m, 2H), 2.41 (s, 3H). ^{13}C NMR (101 MHz, $CDCl_3$) δ 151.52, 146.77, 145.69, 133.01, 132.90, 130.14, 127.25, 127.00, 123.36, 122.99, 121.53, 117.06, 117.01, 70.31, 70.20, 50.14, 21.89. Purity was determined to be 96.3% by using HPLC. HRMS (ESI; m/z). Calcd for C34H34N4O2, $[M + H]^+$, 531.2375; found: 531.2379.

N,N'-((ethane-1,2-diylbis(oxy))bis(ethane-2,1-diyl))bis(acridin-9-amine) (**a13**). Yellow solid, yield 54%. ^{1}H NMR (400 MHz, $CDCl_3$) δ 8.05 (d, *J* = 8.6 Hz, 1H), 7.92 (d, *J* = 8.5 Hz, 1H), 7.47 (t, *J* = 7.3 Hz, 1H), 7.17 (t, *J* = 7.4 Hz, 1H), 3.94 (t, *J* = 6.0 Hz, 1H), 3.81 (t, *J* = *J* = 6.0 Hz, 3.3 Hz, 1H), 3.75 (t, *J* = 1.5 Hz, 1H). ^{13}C NMR (101 MHz, $CDCl_3$) δ 152.61, 146.39, 130.59, 126.33, 123.51, 122.77, 116.63, 70.39, 70.13, 50.29. Purity was determined to be 95.1% by using HPLC. HRMS (ESI; m/z). Calcd for C32H30N4O2, $[M + H]^+$, 503.7911; found: 503.7910.

N^1,N^3-bis(2,7-dimethylacridin-9-yl)propane-1,3-diamine (**a14**). Yellow solid, yield 55%. ^{1}H NMR (400 MHz, DMSO-d6) δ 7.90 (s, 2H), 7.59 (d, *J* = 8.5 Hz, 2H), 7.40 (d, *J* = 8.7 Hz, 2H), 3.94 (t, *J* = 5.9 Hz, 2H), 2.33 (s, 6H), 2.29 – 2.15 (m, 1H). ^{13}C NMR (101 MHz, DMSO-d6) δ 151.96, 144.95, 132.84, 131.68, 126.41, 123.01, 116.07, 47.77, 32.09, 21.72. Purity was determined to be 99.2% by using HPLC. HRMS (ESI; m/z). Calcd for C33H32N4, $[M + H]^+$, 485.2699; found: 485.2712.

N^1,N^3-di(acridin-9-yl)propane-1,3-diamine (**a15**). Yellow solid, yield 42%. ^{1}H NMR (400 MHz, $CDCl_3$) δ 8.15 – 7.88 (m, 4H), 7.59 (s, 2H), 7.25 – 7.11 (m, 2H), 4.08 (t, 2H), 2.33 – 2.19 (m, 2H). ^{13}C NMR (101 MHz, CH_3OD) δ 154.07, 149.10, 131.27, 127.66, 124.75, 123.28, 117.26, 48.70, 33.49. Purity was determined to be 95.1% by using HPLC. HRMS (ESI; m/z). Calcd for C29H24N4, $[M + H]^+$, 429.2073; found: 429.2085.

N^1,N^4-bis(2,7-dimethylacridin-9-yl)butane-1,4-diamine (**a16**). Yellow solid, yield 43%. ^{1}H

NMR (400 MHz, DMSO-d6) δ 8.03 (s, 1H), 7.72 (d, *J* = 8.1 Hz, 1H), 7.44 (d, *J* = 8.7 Hz, 1H), 3.75 (s, 1H), 2.41 (s, 3H), 1.81 (s, 1H). ^{13}C NMR (101 MHz, DMSO-d6) δ 150.54, 147.15, 132.21, 131.60, 128.53, 122.89, 117.09, 50.19, 28.82, 21.91. Purity was determined to be 95.2% by using HPLC. HRMS (ESI; m/z). Calcd for C34H34N4, $[M + H]^+$, 499.2856; found: 499.2853.

N^1,N^4-bis(2-methylacridin-9-yl)butane-1,4-diamine (**a17**). Yellow solid, yield 43%. ^{1}H NMR (400 MHz, $CDCl_3$) δ 8.21 (d, *J* = 8.5 Hz, 1H), 8.03 (s, 1H), 7.72 (s, 1H), 7.67 – 7.63 (m, 1H), 7.55 (t, *J* = 7.4 Hz, 1H), 7.43 (d, *J* = 8.4 Hz, 1H), 7.19 (t, *J* = 7.4 Hz, 1H), 3.78 (t, *J* = 7.0 Hz, 2H), 2.39 (s, 3H), 1.88 – 1.73 (m, 2H). ^{13}C NMR (101 MHz, DMSO) δ 151.56, 147.49, 146.13, 132.69, 131.50, 130.06, 126.90, 126.65, 125.16, 123.29, 122.07, 116.96, 116.86, 50.27, 28.86, 21.80. Purity was determined to be 95.7% by using HPLC. HRMS (ESI; m/z). Calcd for C32H30N4, $[M + H]^+$, 471.2543; found: 471.2561.

N^1,N^5-bis(2,7-dimethylacridin-9-yl)pentane-1,5-diamine (**a18**). Yellow solid, yield 59%. ^{1}H NMR (400 MHz, DMSO-d6) δ 8.05 (s, 2H), 7.74 (d, *J* = 8.0 Hz, 2H), 7.44 (d, *J* = 8.7 Hz, 2H), 3.69 (t, *J* = 7.1 Hz, 2H), 2.43 (s, 6H), 1.77 – 1.60 (m, 2H), 1.48 – 1.36 (m, 1H). ^{13}C NMR (101 MHz, DMSO-d6) δ 150.54, 132.20, 131.63, 131.61, 122.85, 122.78, 117.03, 50.27, 30.92, 24.35, 21.93. Purity was determined to be 99.1% by using HPLC. HRMS (ESI; m/z). Calcd for C35H36N4, $[M + H]^+$, 513.3012; found: 513.3040.

N^1,N^5-bis(2-methylacridin-9-yl)pentane-1,5-diamine (**a19**). Yellow solid, yield 46%. ^{1}H NMR

(400 MHz, $CDCl_3$) δ 8.00 (d, *J* = 8.6 Hz, 2H), 7.92 (d, *J* = 8.8 Hz, 1H), 7.75 (s, 1H), 7.58 (t, *J* = 7.6 Hz, 1H), 7.43 (d, *J* = 8.7 Hz, 1H), 7.25 (t, *J* = 7.6 Hz, 1H), 3.71 (t, *J* = 7.1 Hz, 2H), 2.44 (s, 3H), 1.83 – 1.70 (m, 2H), 1.57 – 1.46 (m, 1H). ^{13}C NMR (101 MHz, $CDCl_3$) δ 151.09, 147.82, 146.83, 132.99, 132.96, 129.99, 128.10, 127.91, 123.04, 122.97, 120.98, 116.33, 116.31, 50.26, 31.13, 24.21, 21.95. Purity was determined to be 95.1% by using HPLC. HRMS (ESI; m/z). Calcd for C33H32N4, $[M + H]^+$, 485.2700; found: 485.2714.

N^1,N^6-bis(2,7-dimethylacridin-9-yl)hexane-1,6-diamine (**a20**). Yellow solid, yield 61%. ^{1}H NMR (400 MHz, DMSO-d6) δ 8.06 (s, 2H), 7.73 (d, *J* = 8.7 Hz, 2H), 7.47 (dd, *J* = 17.7, 10.0 Hz, 2H), 3.68 (t, *J* = 7.1 Hz, 2H), 2.43 (s, 6H), 1.78 – 1.57 (m, 2H), 1.42 – 1.22 (m, 2H). ^{13}C NMR (101 MHz, DMSO-d6) δ 151.00, 146.59, 132.52, 131.73, 127.88, 122.96, 116.74, 50.10, 30.94, 26.55, 21.89. Purity was determined to be 97.8% by using HPLC. HRMS (ESI; m/z). Calcd for C36H38N4, $[M + H]^+$, 527.3079; found: 527.3090.

N^1,N^6-bis(2-methylacridin-9-yl)hexane-1,6-diamine (**a21**). Yellow solid, yield 48%. ^{1}H NMR (400 MHz, $CDCl_3$) δ 8.08 (d, *J* = 8.7 Hz, 1H), 7.96 (d, *J* = 8.7 Hz, 1H), 7.87 (d, *J* = 8.8 Hz, 1H), 7.83 (s, 1H), 7.57 (t, *J* = 7.5 Hz, 1H), 7.41 (d, *J* = 8.7 Hz, 1H), 7.25 (t, *J* = 7.5 Hz, 1H), 3.78 (t, *J* = 6.8 Hz, 2H), 2.44 (s, 3H), 1.81 (s, 2H), 1.46 (s, 2H). ^{13}C NMR (101 MHz, $CDCl_3$) δ 152.12, 146.45, 145.30, 133.53, 132.94, 130.65, 126.40, 126.20, 123.42, 122.86, 121.41, 115.55, 115.48, 50.01, 30.91, 26.40, 21.76. Purity was determined to be 98.0% by using HPLC. HRMS (ESI; m/z). Calcd for C34H34N4, $[M + H]^+$, 499.2856; found: 499.2834.

N^1,N^7-bis(2,7-dimethylacridin-9-yl)heptane-1,7-diamine (**a22**). Yellow solid, yield 52%. ^{1}H NMR (400 MHz, $CDCl_3$) δ 7.99 (d, *J* = 8.8 Hz, 2H), 7.79 (s, 2H), 7.47 (dd, *J* = 8.8, 1.7 Hz, 2H), 3.68 (t, *J* = 7.2 Hz, 2H), 2.52 (s, 6H), 1.80 – 1.65 (m, 2H), 1.52 – 1.33 (m, 3H). ^{13}C NMR (101 MHz, $CDCl_3$) δ 149.75, 147.65, 132.91, 132.17, 129.40, 120.85, 117.35, 50.87, 31.63, 31.58, 26.78, 22.08. Purity was determined to be 97.6% by using HPLC. HRMS (ESI; m/z). Calcd for C37H40N4, $[M + H]^+$, 541.3325; found: 541.3341.

N^1,N^7-bis(2-methylacridin-9-yl)heptane-1,7-diamine (**a23**). Yellow solid, yield 51%. ^{1}H NMR (400 MHz, $CDCl_3$) δ 8.06 (d, *J* = 3.4 Hz, 1H), 8.04 (d, *J* = 3.4 Hz, 1H), 7.98 (d, *J* = 8.8 Hz, 1H), 7.78 (s, 1H), 7.60 (t, *J* = 7.6 Hz, 1H), 7.47 (dd, *J* = 8.8, 1.2 Hz, 1H), 7.30 (t, *J* = 7.6 Hz, 1H), 3.69 (t, *J* = 7.2 Hz, 2H), 2.49 (s, 3H), 1.74 – 1.62 (m, 2H), 1.42 – 1.23 (m, 4H). ^{13}C NMR (101 MHz, $CDCl_3$) δ 150.71, 148.68, 147.78, 132.88, 132.66, 129.59, 129.22, 129.04, 122.98, 122.92, 120.85, 116.81, 116.74, 50.74, 31.56, 28.93, 26.69, 22.07. Purity was determined to be 95.3% by using HPLC. HRMS (ESI; m/z). Calcd for C35H36N4, $[M + H]^+$, 513.3012; found: 513.3030.

N^1,N^7-di(acridin-9-yl)heptane-1,7-diamine (**a24**). Yellow solid, yield 65%. ^{1}H NMR (400 MHz, $CDCl_3$) δ 8.05 (t, *J* = 9.3 Hz, 4H), 7.63-7.56 (m, 2H), 7.32-7.28 (m, 2H), 3.71 (t, *J* = 7.2 Hz, 2H), 1.71 – 1.58 (m, 2H), 1.39 – 1.20 (m, 3H). ^{13}C NMR (101 MHz, $CDCl_3$) δ 151.43, 149.13, 129.96, 129.21, 122.98, 122.77, 116.51, 50.70, 31.56, 28.87, 26.63. Purity was determined to be 97.9% by using HPLC. HRMS (ESI; m/z). Calcd for C33H32N4 (Exact Mass: 484.2627), $[M + Na]^+$,

507.2712; found: 507.2720.

9,9'-(((ethane-1,2-diylbis(oxy))bis(ethane-2,1-diyl))bis(azanediyl))bis(N-(3-(dimethylamino)propyl)-7-methylacridine-2-carboxamide) (**a25**). Yellow solid, yield 33%. ^{1}H NMR (400 MHz, $CDCl_3$) δ 8.90 (s, 1H), 8.77 (s, 1H), 7.88 (d, *J* = 6.6 Hz, 1H), 7.83 (d, *J* = 7.9 Hz, 1H), 7.78 (s, 1H), 7.74 (d, *J* = 8.8 Hz, 1H), 7.39 (d, *J* = 7.3 Hz, 1H), 3.96 (t, *J* = 4.7 Hz, 2H), 3.78 (s, 2H), 3.75 (s, 2H), 3.57 – 3.50 (m, 2H), 2.45 (t, *J* = 6.2 Hz, 2H), 2.41 (s, 3H), 2.26 (s, 6H), 1.80 – 1.71 (m, 2H). ^{13}C NMR (101 MHz, $CDCl_3$) δ 167.00, 157.18, 152.62, 133.60, 132.77, 129.55, 127.67, 126.91, 124.65, 121.90, 119.56, 116.26, 115.71, 115.42, 70.05, 58.44, 58.42, 49.71, 45.25, 40.09, 25.76, 21.83. Purity was determined to be 100% by using HPLC. HRMS (ESI; m/z). Calcd for C46H58N8O4, $[M + H]^+$, 787.4854; found: 787.4875.

9,9'-(((ethane-1,2-diylbis(azanediyl))bis(propane-3,1-diyl))bis(azanediyl))bis(N-(3-(dimethylamino)propyl)-7-methylacridine-2-carboxamide) (**a26**). Yellow solid, yield 44%. ^{1}H NMR (400 MHz, CD_3OD) δ 8.58 (d, *J* = 1.4 Hz, 1H), 7.78 (dd, *J* = 9.0, 1.7 Hz, 1H), 7.62 (s, 1H), 7.53 (d, *J* = 9.0 Hz, 1H), 7.45 (d, *J* = 8.7 Hz, 1H), 7.35 – 7.26 (m, 1H), 3.75 (t, *J* = 6.2 Hz, 2H), 3.34 (t, *J* = 7.1 Hz, 2H), 2.76 – 2.68 (m, 4H), 2.35 – 2.27 (m, 5H), 2.15 (s, 6H), 1.86 – 1.76 (m, 2H), 1.76 – 1.66 (m, 2H). ^{13}C NMR (101 MHz, CD_3OD) δ 167.88, 153.19, 147.94, 146.12, 133.47, 132.31, 127.26, 126.67, 125.76, 125.60, 125.44, 122.19, 115.26, 113.86, 56.95, 49.45, 48.47, 47.83, 44.07, 38.18, 29.55, 26.89, 20.52. Purity was determined to be 96.5% by using HPLC. HRMS (ESI; m/z). Calcd for C48H64N10O2, $[M + H]^+$, 814.3427; found: 814.3414.

dimethyl 9,9'-(((ethane-1,2-diylbis(oxy))bis(ethane-2,1-diyl))bis(azanediyl))bis(7-methylacridine-2-carboxylate) (**a27**). Yellow solid, yield 62%. ^{1}H NMR (400 MHz, $CDCl_3$) δ 8.62 (s, 1H), 7.79 (d, *J* = 8.4 Hz, 1H), 7.64 (d, *J* = 8.3 Hz, 1H), 7.55 (d, *J* = 8.3 Hz, 2H), 7.09 (d, *J* = 7.6 Hz, 1H), 3.95 – 3.86 (m, 4H), 3.82 (s, 3H), 3.81 – 3.76 (m, 2H), 2.23 (s, 3H). ^{13}C NMR (101 MHz, $CDCl_3$) δ 166.64, 152.92, 133.45, 132.43, 129.46, 129.42 (d, *J* = 2.4 Hz), 128.14, 122.79, 122.44, 122.40, 116.52, 115.10, 70.59, 69.96, 52.14, 50.66, 21.59. Purity was determined to be 95.8% by using HPLC. HRMS (ESI; m/z). Calcd for C38H38N4O6, $[M + H]^+$, 647.2846; found: 647.2818.

dimethyl 9,9'-(((ethane-1,2-diylbis(azanediyl))bis(propane-3,1-diyl))bis(azanediyl))bis(7-methylacridine-2-carboxylate) (**a28**). Yellow solid, yield 71%. ^{1}H NMR (400 MHz, $CDCl_3$) δ 8.88 (s, 1H), 8.02 (d, *J* = 9.0 Hz, 1H), 7.80 (dd, *J* = 17.3, 8.8 Hz, 2H), 7.68 (s, 1H), 7.42 (d, *J* = 8.7 Hz, 1H), 3.99 – 3.93 (m, 2H), 3.91 (s, 3H), 3.00 – 2.90 (m, 4H), 2.43 (s, 3H), 1.97 – 1.83 (m, 2H). ^{13}C NMR (101 MHz, $CDCl_3$) δ 167.23, 152.86, 149.91, 148.09, 133.54, 132.24, 129.41, 128.44, 127.87, 127.79, 122.40, 121.81, 115.45, 113.97, 52.12, 50.53, 49.10, 48.63, 29.70, 21.78. Purity was determined to be 100% by using HPLC. HRMS (ESI; m/z). Calcd for C40H44N6O4, $[M + H]^+$, 673.3454; found: 673.3474.

Biophysical and biochemical evaluation experiments

Biochemicals and materials. All oligomers/primers used in this study were purchased from Invitrogen or Sangon, as shown in **Table S1** in Supporting Information. Stock solutions of all the derivatives (10 mM) were prepared using DMSO (10%) or double-distilled deionized water. Further dilutions to working concentrations were carried out with double-distilled deionized water or buffer. All other chemicals or solvents were of analytical grade or better.

Fluorescence resonance energy transfer (FRET) melting assay

FRET melting assay was carried out on a real-time PCR apparatus following previously published procedures. The following fluorescently dual labeled oligonucleotides were used as the FRET probes. FPy33T was prepared as 10 μM solution in 1 × BPES buffer containing 30 mM (KH_2PO_4, K_2HPO_4), 1 mM EDTA, and 100 mM KCl, pH 5.5. FPu22T: 5′-FAM-TGAG GGTGGGTAGGGTGGGTAA-TAMRA-3′, was prepared as 10 μM solution in Tris-HCl buffer (10 mM, pH 7.4) containing 10 mM KCl. F10T: 5′-FAM-dTATAGCTATA-HEG-TATAGCTATA-TAMRA-3′, was prepared as 10 μM solution in Tris-HCl buffer (10 mM, pH 7.4) containing 60 mM KCl. Donor fluorophore FAM is 6-carboxyfluorescein, and acceptor fluorophore TAMRA is 6-carboxytetramethylrhodamine, and HEG linker is [$(-CH_2-CH_2-O-)_6$]. These oligonucleotides were thermally annealed. Fluorescence melting curves were determined with a Roche Light Cycler 2 real-time PCR instrument, using a total reaction volume of 20 μL, with 0.2 μM dual labeled oligonucleotide with or without compounds for FPy33T, FPu22T, F10T, respectively. Fluorescence readings with excitation at 470 nm and detection at 530 nm were taken at intervals of 1 °C over the range 37-99 °C, with a

constant temperature being maintained for 30 s prior to each reading to ensure a stable value. The melting of i-motif, G-quadruplex and duplex were monitored in the absence or presence of various concentrations of compounds. Final analysis of the data was carried out using Origin8.0 (OriginLab Corp.).

Surface Plasmon Resonance (SPR) measurement

SPR measurement was performed on a ProteOn XPR36 Protein Interaction Array system (Bio-Rad Laboratories, Hercules, CA) using a Neutravidin-coated GLH sensor chip. For immobilization, all DNA samples were biotinylated and attached to a reptavidin-coated sensor chip. Oligomer 5′-biotin Py33 was diluted to 1 μM in running buffer (20 mM 2-(4-morpholino)ethanesulfonic acid, pH 5.8, 100 mM KCl and 0.05% Tween-20), and 5′-biotin Pu27 and 5′-biotin duplex DNA were diluted to 1 μM in running buffer (Tris-HCl 50 mM, pH 7.4, 100 mM KCl). The DNA samples were then captured (1000 RU) in flow cells, and a blank cell was set as a control. Different ligand-containing solutions were prepared with the running buffer through serial dilutions from stock solution (10 mM in DMSO). Six concentrations were injected simultaneously at a flow rate of 25 mL/ min for 260 s of association phase, followed with 300 s of dissociation phase at 25 ^{o}C. The GLH sensor chip was regenerated with short injection of 50 mM NaOH between consecutive measurements. The final graphs were obtained by subtracting blank sensorgrams of i-motif, G-quadruplex or duplex DNA. Data were analyzed with ProteOn manager software.

CD experiments

CD experiments were performed on a Chirascan circular dichroism spectrophotometer (Applied Photophysics). A quartz cuvette with 4 mm path length was used for the spectra recorded over a wavelength range of 230-400 nm at 1 nm bandwidth, 1 nm step size, and 0.5 s per point. The oligomer c-*myc* Py33 or Pu27 was diluted from stock to the required concentration (1 μM) in the absence or presence of compounds (Py33: 1 × BPES buffer, pH 5.5 or 6.8; Pu27: 10 mM Tris-HCl buffer, pH 7.4), and then annealed by heating at 95 °C for 5 min, gradually cooled to room temperature, and stored at 4 °C overnight. Spectra were recorded three times over a wavelength range of 230-350 nm, averaged, smoothed, and baseline corrected to remove signal contribution from buffer. Final analysis of the data was carried out using Origin 8.0 (OriginLab Corp.).

For melting studies, the i-motif or G-quadruplex oligomers of c-*myc*, *bcl-2*, *c-kit,* PDGF, telomere and VEGF were diluted from stock to 1 μM in the absence or presence of **a9**, **a11** and **a26** (i-motif: 1 × BPES buffer, pH 6.4; G-quadruplex: 10 mM Tris-HCl buffer, 5 mM KCl, pH 7.4), and then annealed by heating at 95 °C for 5 min followed by gradual cooling to room temperature. Thermal melting was monitored at 260 nm at the heating rate of 1 °C/min. The melting temperatures were determined through curve fitting of melting profiles using GraphPad Prism software.

^{1}H NMR

The NMR samples were prepared in 10%/90% D_2O/H_2O solution. The oligomer c-*myc* Py33 or Pu27 was diluted from stock to 0.5 mM in the absence or presence of **a9** (Py33: 1 × BPES buffer,

pH 6.4; Pu27: 10 mM Tris-HCl buffer, pH 7.4), and then annealed by heating at 95 °C for 5 min, gradually cooled to room temperature. The stock solution of compound was dissolved in d_6-DMSO. One-dimensional ^{1}H NMR titration experiments were performed on a Bruker DRX-600 MHz spectrometer at temperatures of 25 °C, and the water signal was suppressed in the experiment.

Isothermal titration calorimetry (ITC)

ITC experiments were performed using a VP-ITC titration calorimeter (MicroCal, Northampton, MA). Before loading, the solutions were thoroughly degassed. The reference cell was filled with the degassed buffer. The preformed DNA (500 μM Pu27 or 200 μM Py33) was kept in the sample cell, and a syringe with a volume of 300 μL was filled with the ligand **a9** (Pu27: 50 μM **a9**, Py33: 20 μM **a9**) in the same buffer. The ligand solution was added sequentially in 10 μL aliquots (for a total of 28 injections with a duration of 10 s each) at 4 min intervals at 20 °C. In control experiments, the heats of dilution were determined in parallel experiments by injecting ligand solution of the same concentration in the same buffer. The respective heats of dilution were subtracted from the corresponding binding experiments prior to curve fitting. The thermograms (integrated heat/injection data) obtained in the ITC experiments were fitted with an appropriate model in Origin 7.0.

Native PAGE experiments

Native PAGE experiments were carried out in 1 × TBE buffer (pH 6.8). The oligomer c-*myc*

Py33 was diluted from stock to the required concentration (3 μM) in 1 × BPES buffer (pH 6.8) in the absence or presence of different concentrations of compound **a9** and **a26**, and then annealed by heating at 95 °C for 5 min. Then these oligomers were gradually cooled to room temperature, and incubated at 4 °C overnight. Electrophoresis was carried out by using 20% acrylamide (pH 6.6) at 140 V for 5 h at 5 °C. The gels were then silver-stained.

Cell culture

Human melanoma cell line A375, human squamous cervical cancer cell line Hela, human lung adenocarcinoma cell line A549, human bone osteosarcoma epithelial cell line U2OS, human colon cancer cell line HCT116, human cervical cancer cell line SiHa, and human hepatocellular carcinoma cell line HuH7 were purchased from China Center for Type Culture Collection in Wuhan. The cell lines were maintained in RPMI-1640 or DMEM medium supplemented with 10% fetal calf serum at 37 °C in a humidified atmosphere with 5% CO_2.

MTT cytotoxicity assay

A375, Hela, A549, U2OS, HCT-116, SiHa, and HuH7 cells were seeded on 96-well plates (5.0×10^3 per well) with 100 μL of culture medium and incubated for 12 h at 37 °C in a humidified atmosphere with 5% CO_2, respectively. The cells were incubated in the presence or absence of the indicated concentrations of compound**s,** and the control group was administered the same volume of DMSO. After incubation for 48 h, 20 μL of 2.5 mg/mL methyl thiazolyl tetrazolium (MTT) solution was added to each well and further incubated for 4 h. The cells in each well were then

treated with dimethyl sulfoxide (200 μL) after the culture medium was siphoned off and the absorbance was recorded at 570 nm. All drug doses were parallel tested in triplicate, and the cytotoxicity was evaluated based on the percentage of cell survival in dose dependent manner deducting the negative control. The final IC_{50} values were calculated by using the Graph Pad Prism 6.

Dual-Luciferase reporter assay

In this assay, 200 ng of constructed psiCHECK2 luciferase plasmid (Promega, USA) containing c-*myc* wild type, mutant or deleted promoters were transfected into SiHa cells by using Lipofectamine 3000 (Invitrogen, USA). After 8 h, compounds were added to the cells. The cells were incubated at 37 °C with CO_2 for 48 h, and the transfected cells were first washed with ice-cold 1 × PBS buffer to reduce the background signals from the medium. Luciferase assays were subsequently performed according to the manufacturer's instructions using the dual-luciferase assay system (Promega, USA). After a 3 s delay, secreted luciferase signals were collected for 10 s using a microplate reader (Molecular Devices, Flex Station 3, USA). The quantification was performed using a multimode reader (Molecular Devices). The secreted Renilla luciferase activity was normalized to the firefly luciferase activity.

RNA extraction and reverse transcription polymerase chain reaction (RT-PCR)

SiHa cells were seeded in 6-well plate (2×10^5 cells/well), and incubated for 12 h at 37 ^oC in a humidified atmosphere with 5% CO_2. The cells were incubated in the presence or absence of

different concentrations of **a9** and **a26,** and the control group was administered the same volume of DMSO. After incubation for 24 h, the harvested cells were washed with 1 × PBS (pH 7.4) and lysed in a TRIzol solution. The total RNA was extracted according to the protocol supplied by the Takara Company, and eluted with distilled, deionized water containing 0.1% diethyl pyrocarbonate (DEPC) to give a final volume of 30 μL. RNA was quantified spectrophotometrically. The total RNA was used as a template for reverse transcription according to the following protocol: each 20 μL reaction contained 1×M-MLV buffer, 500 μM dNTP, 100 pmol oligo dT18 primer, 100 units of M-MLV reverse transcriptase, DEPC-H_2O, and 1.5 μg total RNA. The mixtures were incubated at 42 °C for 60 min for reverse transcription, and then at 70 °C for 15 min. PCR was performed according to the following protocol: each 20-μL reaction contained 1× PCR buffer, 500 μM dNTPs, 0.2 μM primer pairs, 1 unit *Taq* polymerase, 0.1% DEPC-H_2O and 2 μL cDNA template. The reactions were performed in a Master-cycler Personal (Eppendorf) according to the following protocol: 95 °C for 5 min, 30 cycles of 95 °C for 1 min, 58 °C for 30 s, and 72 °C for 1 min. The amplified products were separated on 1.2% agarose gel, and photographed using a Gel Doc 2000 Imager System.

RNA stability assay

SiHa cells were seeded in 6-well plate (2×10^5/well) and incubated for 24 h at 37 °C in a humidified atmosphere with 5% CO_2. The cells were incubated in the presence of 5 μg/mL Actinomycin D or 5 μg/mL Actinomycin D plus 2.5 μM **a9**. Total RNA was extracted according to the protocol supplied by the Takara Company at the indicated time points following the

addition of Actinomycin D. The reverse transcription and PCR process were performed using normal RT-PCR methods. The transcript turnover rates were then calculated based on non-linear fitting one phase exponential decay curves using GraphPad Prism software, and were generally expressed as times to 50% mRNA decay for each experiment.

Western blot

After SiHa cells were taken board for each well of 2×10^5 and then treated with different concentrations of **a9** and **a26** for 24 h, the cells harvested from each well of culture plates were lysed in 200 μL of protein extraction buffer consisting of 1 mM PMSF for 30 min. The suspension was centrifuged at 10,000 rpm at 4 °C for 15 min, and the protein content of supernatant was measured by using BCA assay. The same amount of protein for each sample was loaded onto 8% polyacrylamide gel, and then transferred to a microporous polyvinylidene difluoride (PVDF) membrane. Western blotting was performed by using anti-c-MYC and anti-β-actin (cell signaling technology) antibodies, as well as horseradish peroxidase-conjugated anti-rabbit secondary antibody. Protein bands were visualized by using chemiluminescence substrate.

Colony formation assay

SiHa cells were subsequently seeded in 6-well culture plates (500/well) for a 24 h pre-culture at 37 ^{o}C in a humidified atmosphere with 5% CO_2, and then treated with **a9** at different concentrations for 9 days. The cells were washed with 1 × PBS and fixed with ice cold methanol for 10 min, followed by the addition of 0.5% crystal violet solution for 30 min to observe the

colony formation. Finally, the plates were washed with water, dried and photographed.

Annexin V-FITC apoptosis detection

SiHa cells were seeded in 6-well plate (2×10^5/well) and incubated for 24 h at 37 °C in a humidified atmosphere with 5% CO_2. After incubated in the presence of different concentrations of **a9** and the control group was administered the same volume of DMSO for 24 h, the SiHa cells were washed with PBS, centrifuged and re-suspended in Annexin V-FITC solution for 15 min at room temperature in dark. After centrifuged for 5 min, the cells were then re-suspended in Annexin V-FITC solution and mixed with PI staining solution for 10 min at 2-5 °C in dark. Then, the cells were analyzed by using flow cytometry with an Epics Elite flow cytometer (Beckman Coulter, USA).

Cell cycle analysis

SiHa cells were seeded in 6-well plate (2×10^5/well) and incubated for 24 h at 37 °C in a humidified atmosphere with 5% CO_2. After incubated in the presence of different concentrations of **a9** and the control group was administered the same volume of DMSO for 24 h, the SiHa cells were then washed in PBS. The cells were harvested and fixed in ice cold 70% ethanol overnight. The cells were centrifuged and re-suspended in 1 mL of PBS containing 20 μg/mL of RNase A at 37 °C for 30 min. The cells were then incubated with the DNA staining solution PI solution, and flow cytometry analysis was carried out using an Epics Elite flow cytometry (Beckman Coulter, Epics XL) measured at 488 nm. The data were analyzed by using EXPO32 ADC analysis

software.

Evaluation of in vivo anti-tumor activity

BALB/c female nude mice were obtained from the laboratory animal center of Sun Yat-sen University. All procedures were approved by the Animal Care and Use Committee of Sun Yat-sen University and conformed to the legal mandates and national guidelines for the care and maintenance of laboratory animals. SiHa cells were harvested, pelleted through centrifugation at 1,000 rpm for 5 min, and resuspended in sterile serum-free medium without EDTA. The cells (1×10^7 in 100 μL) were then subcutaneously implanted into the underarm regions of five mice. After the tumors grew to almost 1,000 mm^3, the tumor tissues were removed and divided. Then, the divided tissues were implanted into the underarm of 18 mice. These mice were separated into three groups: negative control, **a9**-treated, and positive control (cisplatin-treated). **a9**, cisplatin, and saline were administered by ip injection to athymic nude mice with human tumor xenografts established using SiHa cervical cancer cells. Mice were injected ip once two days for 18 days. The positive control group received cisplatin at a dose of 0.2 mg/kg, and **a9** was similarly administered to mice at a dose of 15 mg/kg. After treatment of the animals for 18 days, the animals were sacrificed, and organs of the mice were collected and weighed.

ASSOCIATED CONTENT

Supporting Information

Additional experimental results, ^1H and ^{13}C NMR spectra, and HRMS spectra, as well as HPLC

data for final compounds (PDF) are available free of charge via the Internet at http://pubs.acs.org.

Molecular Formula Strings (CSV).

C-myc promoter G-quadruplex (PDB ID: 2L7V) or a model tetrameric i-motif (PDB ID: 1YBL) in complex with docking pose of compound **a9** (PDB): author will release the atomic coordinates upon article publication.

AUTHOR INFORMATION

Corresponding Author

Ding Li, phone and fax: 8620 3994 3058; E-mail: liding@mail.sysu.edu.cn;

Bing Shu, phone and fax: 8620 3935 2129; E-mail: shubing@gdpu.edu.cn.

ACKNOWLEDGMENTS

We thank National Natural Science Foundation of China (Grant 21977123), Guangdong Basic and Applied Basic Research Foundation (Grant 2019A1515011074), Youth Innovation Talents Project of Colleges and Universities in Guangdong Province (Grant 51340208), Natural Science Foundation of Guangdong Province (Grants 2017A030313089, 2017A030308003), and Guangdong Provincial Key Laboratory of Construction Foundation (2017B030314030) for financial support of this study.

ABBREVIATIONS

CD, circular dichroism; EMSA, electrophoretic mobility shift assay; FRET, fluorescence resonance energy transfer; ITC, isothermal titration calorimetry; NHE III_1, nuclease hypersensitive

element III_1; SPR, surface plasmon resonance.

REFERENCES

1. Hsu, T. Y.; Simon, L. M.; Neill, N. J.; Marcotte, R.; Sayad, A.; Bland, C. S.; Echeverria, G. V.; Sun, T.; Kurley, S. J.; Tyagi, S.; Karlin, K. L.; Dominguez-Vidana, R.; Hartman, J. D.; Renwick, A.; Scorsone, K.; Bernardi, R. J.; Skinner, S. O.; Jain, A.; Orellana, M.; Lagisetti, C.; Golding, I.; Jung, S. Y.; Neilson, J. R.; Zhang, X. H.; Cooper, T. A.; Webb, T. R.; Neel, B. G.; Shaw, C. A.; Westbrook, T. F., The spliceosome is a therapeutic vulnerability in MYC-driven cancer. *Nature* **2015,** *525*, 384-388.

2. Chen, B. J.; Wu, Y. L.; Tanaka, Y.; Zhang, W., Small molecules targeting c-Myc oncogene: promising anti-cancer therapeutics. *Int J Biol Sci* **2014,** *10*, 1084-1096.

3. Cui, F. M.; Sun, X. J.; Huang, C. C.; Chen, Q.; He, Y. M.; Zhang, S. M.; Guan, H.; Song, M.; Zhou, P. K.; Hou, J., Inhibition of c-Myc expression accounts for an increase in the number of multinucleated cells in human cervical epithelial cells. *Oncol Lett* **2017,** *14*, 2878-2886.

4. Chi V. Dang, L. M. S. R., Eileen Emison, Sunkyu Kim, Qing Li, Julia E. Prescott, Diane Wonsey, and Karen Zeller, Function of the c-Myc oncogenic transcription factor. *Experimental Cell Research* **1999,** *253*, 63–77.

5. Lin, C. Y.; Loven, J.; Rahl, P. B.; Paranal, R. M.; Burge, C. B.; Bradner, J. E.; Lee, T. I.; Young, R. A., Transcriptional amplification in tumor cells with elevated c-Myc. *Cell* **2012,** *151*, 56-67.

6. Wright, E. P.; Day, H. A.; Ibrahim, A. M.; Kumar, J.; Boswell, L. J.; Huguin, C.; Stevenson, C. E.; Pors, K.; Waller, Z. A., Mitoxantrone and analogues bind and stabilize i-motif forming DNA sequences. *Sci Rep* **2016,** *6*, 39456-39462.

7. Dorasamy, M. S.; Choudhary, B.; Nellore, K.; Subramanya, H.; Wong, P. F., Dihydroorotate dehydrogenase inhibitors target c-myc and arrest melanoma, myeloma and lymphoma cells at S-phase. *J Cancer* **2017,** *8*, 3086-3098.

8. Oh, E. T.; Kim, C. W.; Kim, H. G.; Lee, J. S.; Park, H. J., Brusatol-mediated inhibition of c-myc increases hif-1alpha degradation and causes cell death in colorectal cancer under hypoxia. *Theranostics* **2017,** *7*, 3415-3431.

9. Akinyeke, T.; Weber, S. J.; Davenport, A. T.; Baker, E. J.; Daunais, J. B.; Raber, J., Effects of alcohol on c-Myc protein in the brain. *Behav Brain Res* **2017,** *320*, 356-364.

10. Floor, R. J.; Wijma, H. J.; Jekel, P. A.; Terwisscha van Scheltinga, A. C.; Dijkstra, B. W.; Janssen, D. B., X-ray crystallographic validation of structure predictions used in computational design for protein stabilization. *Proteins* **2015,** *83*, 940-951.

11. Jung, K. Y.; Wang, H.; Teriete, P.; Yap, J. L.; Chen, L.; Lanning, M. E.; Hu, A.; Lambert, L. J.; Holien, T.; Sundan, A.; Cosford, N. D. P.; Prochownik, E. V.; Fletcher, S., Perturbation of the c-Myc–Max protein–protein interaction via synthetic α-helix mimetics. *Journal of Medicinal Chemistry* **2015,** *58*, 3002-3024.

12. Gonzalez, V.; Hurley, L. H., The c-MYC NHE III(1): function and regulation. *Annu Rev*

Pharmacol Toxicol **2010,** *50*, 111-129.

13. Dai, J.; Hatzakis, E.; Hurley, L. H.; Yang, D., I-motif structures formed in the human c-MYC promoter are highly dynamic--insights into sequence redundancy and I-motif stability. *PLoS One* **2010,** *5*, 11647-11654.

14. Kaiser, C. E.; Van Ert, N. A.; Agrawal, P.; Chawla, R.; Yang, D.; Hurley, L. H., Insight into the complexity of the i-motif and G-quadruplex DNA structures formed in the kras promoter and subsequent drug-induced gene repression. *J Am Chem Soc* **2017,** *139*, 8522-8536.

15. Kang, H. J.; Kendrick, S.; Hecht, S. M.; Hurley, L. H., The transcriptional complex between the BCL2 i-motif and hnRNP LL is a molecular switch for control of gene expression that can be modulated by small molecules. *J Am Chem Soc* **2014,** *136*, 4172-4185.

16. Ou, T. M.; Lin, J.; Lu, Y. J.; Hou, J. Q.; Tan, J. H.; Chen, S. H.; Li, Z.; Li, Y. P.; Li, D.; Gu, L. Q.; Huang, Z. S., Inhibition of cell proliferation by quindoline derivative (SYUIQ-05) through its preferential interaction with c-myc promoter G-quadruplex. *J Med Chem* **2011,** *54*, 5671-5679.

17. Ruan, J.; Mouveaux, T.; Light, S. H.; Minasov, G.; Anderson, W. F.; Tomavo, S.; Ngo, H. M., The structure of bradyzoite-specific enolase from Toxoplasma gondii reveals insights into its dual cytoplasmic and nuclear functions. *Acta Crystallogr D Biol Crystallogr* **2015,** *71*, 417-426.

18. Biffi, G.; Tannahill, D.; McCafferty, J.; Balasubramanian, S., Quantitative visualization of DNA G-quadruplex structures in human cells. *Nat Chem* **2013,** *5*, 182-186.

19. Liu, L.; Kim, B. G.; Feroze, U.; Macgregor, R. B., Jr.; Chalikian, T. V., Probing the ionic

atmosphere and hydration of the c-myc i-motif. *J Am Chem Soc* **2018,** *140*, 2229-2238.

20. Sutherland, C.; Cui, Y.; Mao, H.; Hurley, L. H., A mechanosensor mechanism controls the G-quadruplex/i-motif molecular switch in the myc promoter NHE III1. *J Am Chem Soc* **2016,** *138*, 14138−14151.

21. Li, H.; Hai, J.; Zhou, J.; Yuan, G., The formation and characteristics of the i-motif structure within the promoter of the c-myb proto-oncogene. *J Photochem Photobiol B* **2016,** *162*, 625-632.

22. Wright, E. P.; Huppert, J. L.; Waller, Z. A. E., Identification of multiple genomic DNA sequences which form i-motif structures at neutral pH. *Nucleic Acids Res* **2017,** *45*, 2951-2959.

23. Cui, J.; Waltman, P.; Le, V. H.; Lewis, E. A., The effect of molecular crowding on the stability of human c-MYC promoter sequence I-motif at neutral pH. *Molecules* **2013,** *18*, 12751-12767.

24. Garabedian, A.; Butcher, D.; Lippens, J. L.; Miksovska, J.; Chapagain, P. P.; Fabris, D.; Ridgeway, M. E.; Park, M. A.; Fernandez-Lima, F., Structures of the kinetically trapped i-motif DNA intermediates. *Phys Chem Chem Phys* **2016,** *18*, 26691-26702.

25. Zhou, J.; Wei, C.; Jia, G.; Wang, X.; Feng, Z.; Li, C., Formation of i-motif structure at neutral and slightly alkaline pH. *Mol Biosyst* **2010,** *6*, 580-586.

26. Reilly, S. M.; Lyons, D. F.; Wingate, S. E.; Wright, R. T.; Correia, J. J.; Jameson, D. M.; Wadkins, R. M., Folding and hydrodynamics of a DNA i-motif from the c-MYC promoter

determined by fluorescent cytidine analogs. *Biophys J* **2014,** *107*, 1703-1711.

27. Zeraati, M.; Langley, D. B.; Schofield, P.; Moye, A. L.; Rouet, R.; Hughes, W. E.; Bryan, T. M.; Dinger, M. E.; Christ, D., I-motif DNA structures are formed in the nuclei of human cells. *Nat Chem* **2018,** *10*, 631-637.

28. Dzatko, S.; Krafcikova, M.; Hansel-Hertsch, R.; Fessl, T.; Fiala, R.; Loja, T.; Krafcik, D.; Mergny, J. L.; Foldynova-Trantirkova, S.; Trantirek, L., Evaluation of the stability of DNA i-motifs in the nuclei of living mammalian cells. *Angew Chem Int Ed Engl* **2018,** *57*, 2165-2169.

29. Takahashi, S.; Brazier, J. A.; Sugimoto, N., Topological impact of noncanonical DNA structures on Klenow fragment of DNA polymerase. *Proc Natl Acad Sci U S A* **2017,** *114*, 9605-9610.

30. Qin, T.; Liu, K.; Song, D.; Yang, C.; Su, H., Porphyrin bound to i-motifs: intercalation versus external groove binding. *Chem Asian J* **2017,** *12*, 1578-1586.

31. Oleg Yu. Fedoroff, A. R., Violetta V. Chemeris and Laurence H. Hurley, TMPYP4-cationic porphyrins promote the formation of i-motif DNA and bind peripherally by a nonintercalative mechanism. *Biochemistry* **2000,** *39*, 15083-15090.

32. Debnath, M.; Ghosh, S.; Chauhan, A.; Paul, R.; Bhattacharyya, K.; Dash, J., Preferential targeting of i-motifs and G-quadruplexes by small molecules. *Chem Sci* **2017,** *8*, 7448-7456.

33. Shu, B.; Cao, J.; Kuang, G.; Qiu, J.; Zhang, M.; Zhang, Y.; Wang, M.; Li, X.; Kang, S.; Ou, T. M.; Tan, J. H.; Huang, Z. S.; Li, D., Syntheses and evaluation of new acridone derivatives for

selective binding of oncogene c-myc promoter i-motifs in gene transcriptional regulation. *Chem Commun (Camb)* **2018,** *54*, 2036-2039.

34. Wang, L.; Wu, Y.; Chen, T.; Wei, C., The interactions of phenanthroline compounds with DNAs: preferential binding to telomeric quadruplex over duplex. *Int J Biol Macromol* **2013,** *52*, 1-8.

35. Alberti, P.; Ren, J.; Teulade-Fichou, M. P.; Guittat, L.; Riou, J. F.; Chaires, J.; Helene, C.; Vigneron, J. P.; Lehn, J. M.; Mergny, J. L., Interaction of an acridine dimer with DNA quadruplex structures. *J Biomol Struct Dyn* **2001,** *19*, 505-513.

36. Phanstiel, O. t.; Kaur, N.; Delcros, J. G., Structure-activity investigations of polyamine-anthracene conjugates and their uptake via the polyamine transporter. *Amino Acids* **2007,** *33*, 305-313.

37. Poulin, R.; Casero, R. A.; Soulet, D., Recent advances in the molecular biology of metazoan polyamine transport. *Amino Acids* **2012,** *42*, 711-723.

38. Xie, S.; Wang, J.; Zhang, Y.; Wang, C., Antitumor conjugates with polyamine vectors and their molecular mechanisms. *Expert Opin Drug Deliv* **2010,** *7*, 1049-1061.

39. Kendrick, S.; Kang, H. J.; Alam, M. P.; Madathil, M. M.; Agrawal, P.; Gokhale, V.; Yang, D.; Hecht, S. M.; Hurley, L. H., The dynamic character of the BCL2 promoter i-motif provides a mechanism for modulation of gene expression by compounds that bind selectively to the alternative DNA hairpin structure. *J Am Chem Soc* **2014,** *136*, 4161-4171.

40. Brown, R. V.; Wang, T.; Chappeta, V. R.; Wu, G.; Onel, B.; Chawla, R.; Quijada, H.; Camp, S. M.; Chiang, E. T.; Lassiter, Q. R.; Lee, C.; Phanse, S.; Turnidge, M. A.; Zhao, P.; Garcia, J. G. N.; Gokhale, V.; Yang, D.; Hurley, L. H., The consequences of overlapping G-quadruplexes and i-motifs in the platelet-derived growth factor receptor beta core promoter nuclease hypersensitive element can explain the unexpected effects of mutations and provide opportunities for selective targeting of both structures by small molecules to downregulate gene expression. *J Am Chem Soc* **2017,** *139*, 7456-7475.

41. Li, X.; Peng, Y.; Ren, J.; Qu, X., Carboxyl-modified single-walled carbon nanotubes selectively induce human telomeric i-motif formation. *Proc Natl Acad Sci U S A* **2006,** *103*, 19658-19663.

42. Peng, Y.; Li, X.; Ren, J.; Qu, X., Single-walled carbon nanotubes binding to human telomeric i-motif DNA: significant acceleration of S1 nuclease cleavage rate. *Chem Commun (Camb)* **2007**, 5176-5178.

43. Zhao, C.; Ren, J.; Qu, X., Single-walled carbon nanotubes binding to human telomeric i-motif DNA under molecular-crowding conditions: more water molecules released. *Chemistry* **2008,** *14*, 5435-5439.

44. Su, L.; Zheng, H.; Li, Z.; Qiu, J.; Chen, S.; Liu, J.; Ou, T. M.; Tan, J. H.; Gu, L. Q.; Huang, Z. S.; Li, D. Mechanistic studies on the anticancer activity of 2,4-disubstituted quinazoline derivative. *Biochim Biophys Acta* **2014,** 1840, 3123-3130.

45. Chen, Y.; Qu, K.; Zhao, C.; Wu, L.; Ren, J.; Wang, J.; Qu, X., Insights into the biomedical

effects of carboxylated single-wall carbon nanotubes on telomerase and telomeres. *Nat Commun* **2012,** *3*, 1074-1086.

46. Lian, Q.; Lai, W. S.; Stumpo, D. J.; Blackshear, P. J. Measurement of mRNA decay in mouse embryonic fibroblasts. *Bio-protocol* **2016**, *6*, e1858.

47. Brown, R. V.; Danford, F. L.; Gokhale, V.; Hurley, L. H.; Brooks, T. A., Demonstration that drug-targeted down-regulation of MYC in non-Hodgkins lymphoma is directly mediated through the promoter G-quadruplex. *J Biol Chem* **2011,** *286*, 41018-41027.

48. Liu, H. Y.; Chen, A. C.; Yin, Q. K.; Li, Z.; Huang, S. M.; Du, G.; He, J. H.; Zan, L. P.; Wang, S. K.; Xu, Y. H.; Tan, J. H.; Ou, T. M.; Li, D.; Gu, L. Q.; Huang, Z. S., New disubstituted quindoline derivatives inhibiting burkitt's lymphoma cell proliferation by impeding c-myc transcription. *J Med Chem* **2017,** *60*, 5438-5454.

49. Zeng, D. Y.; Kuang, G. T.; Wang, S. K.; Peng, W.; Lin, S. L.; Zhang, Q.; Su, X. X.; Hu, M. H.; Wang, H.; Tan, J. H.; Huang, Z. S.; Gu, L. Q.; Ou, T. M., Discovery of novel 11-triazole substituted benzofuro[3,2-b]quinolone derivatives as c-myc G-quadruplex specific stabilizers via click chemistry. *J Med Chem* **2017,** *60*, 5407-5423.

50. Boddupally, P. V.; Hahn, S.; Beman, C.; De, B.; Brooks, T. A.; Gokhale, V.; Hurley, L. H., Anticancer activity and cellular repression of c-MYC by the G-quadruplex-stabilizing 11-piperazinylquindoline is not dependent on direct targeting of the G-quadruplex in the c-MYC promoter. *J Med Chem* **2012,** *55*, 6076-6086.

51. Brooks, T. A.; Hurley, L. H., Targeting MYC expression through G-quadruplexes. *Genes Cancer* **2010,** *1*, 641-649.

52. Rodriguez, R.; Miller, K. M.; Forment, J. V.; Bradshaw, C. R.; Nikan, M.; Britton, S.; Oelschlaegel, T.; Xhemalce, B.; Balasubramanian, S.; Jackson, S. P. Small-molecule–induced DNA damage identifies alternative DNA structures in human genes. *Nature chemical biology* **2012,** 8, 301-310.

53. Hoffman, B.; Liebermann, D. A., The proto-oncogene c-myc and apoptosis. *Oncogene* **1998,** *17*, 3351-3357.

54. Obaya, A. J.; Mateyak, M. K.; Sedivy, J. M., Mysterious liaisons: the relationship between c-Myc and the cell cycle. *Oncogene* **1999,** *18*, 2934-2941.

Table of Contents graphic